Light distribution in tissue : a review of four methods to determine optical parameters

Splinter, Robert

Award date:
1987

University of Technology Eindhoven,

Eindhoven, The Netherlands.

Technische Universiteit Eindhoven

Faculteit der Technische Natuurkunde

Vakgroep: Analyse van Fysische Meetmethoden

Light distribution in tissue, A review of four methods to determine optical parameters.

Robert Splinter

Afstudeerwerk verricht aan het Sint Joseph Ziekenhuis te Eindhoven.

datum	juli 1987
afstudeerdocent	Prof.dr. J.A. Poulis
kontaktpersoon	dr.ir. C.H. Massen
begeleider St. Joseph ziekenhuis	dr.ir. M.J.C. van Gemert

Acknowledgement

It gives me great pleasure to acknowledge the help and cooperation I have received from many persons and organisations during last years research.
First of all "Het Koninklijk Instituut voor Ingenieurs" (Kivi) whom also made it possible for me to attend the workshop on "Laser-tissue interaction" at the University of Texas at Austin, Texas, U.S.A..
Thanks to dr. A.J. Welch, Wai-Fung Cheong and Jerry LeCarpentier of the University of Texas for assisting me by word and deed. To Scott Prahl for letting me use his computer program and to the University of Texas for their hospitality.
Also thanks to dr. Willem Star and Hans Marijnissen of the Rotterdam Radiotherapeutic Institute, Rotterdam, The Netherlands, for their kind help and advise. And Pascal Storchi for letting me use his computer program.
I want to thank Rian Becker, who has done most of the typing for this report.
I also wish to thank my parents for their support in my study.
And I also want to thank everyone else who assisted me during the past year.

CONTENTS

SAMENVATTING.

De sterke groei van de medische toepassingen van lasers vraagt om een betere kennis van de optische parameters van weefsel. De optische parameters zijn absorptie- en verstrooiings coefficient en verstrooiings anisotropy factor. Tot op heden is de kennis van de optische parameters van weefsel beperkt. Tevens zijn de methoden ter bepaling van de optische parameter slechts kort geleden ontwikkeld, met tot heden onbekende nauwkeurigheid.
In dit verslag volgt een vergelijkend onderzoek van een viertal methoden die op het ogenblik bekend zijn voor de bepaling van optische parameters, aan de hand van mengsels van verstrooiende en absorberende stoffen (phantomen). De volgende methoden zijn onderzocht: (1) Enkele integrerende bol en (2) dubbele integrerende bol, gebruik makend van gecollimeerde en diffuse transmissie en diffuse reflectie metingen. (3) Lichtverdelings metingen in een groot phantom en (4) hoek afhankelijke transmissie door een plan parallel medium met de goniometer. Lichtverdelings theorie wordt beschreven met de stralings-transport vergelijking. De enkele en dubbele bol metingen vertonen goede overeenkomsten met de excate waarden van de phantomen voor absorptie coefficient groter dan 0,01 mm^{-1}, maar niet voor de verstrooiings coefficient en de verstrooiings anisotropy factor wat waarschijnlijk te wijten is aan de gecollimeerde verzwakkings metingen. De intensiteit in het reservoir met phantoom wordt gemeten met een isotrope detector en vergeleken met computer berekeningen met een programma van Scott Prahl van de Universiteit van Texas, Austin, U.S.A., waarbij gebruik gemaakt wordt van parameter aanpassing om de optische parameters te bepalen. Voor kleine bundel diameter wijken computer-berekeningen af van de experimentele isodose kurven. Dit wordt waarschijnlijk veroorzaakt doordat voor deze situatie de diffuse benadering niet meer geldig is. Deze methode vereist een grote hoeveelheid medium en verscheidene combinaties van optische parameters kunnen dezelfde lichtverdeling geven. De goniometer bepaald de hoekafhankelijke transmissie door een troebele laag. Computer simulatie door Pascal Storchi van de Daniel den Hoed Kliniek in Rotterdam wordt gebruikt om de experimentele resultaten te interpreteren. De experimenteel verkregen kurven wijken af van de berekende kurven. Dit wordt waarschijnlijk veroorzaakt doordat het licht niet volledig diffuus is in de laag, waardoor niet aan de theoretische eis voor de diffusie benadering voldaan is.

SUMMARY.

The strong expansion of the medical applications of lasers demands for a better knowledge of the optical parameters of tissues. The optical parameters are absorption and scattering coefficients and scattering anisotropy factor. So far little is known about the optical parameters of tissues. Methods to determine optical parameters have only recently been developed, with as yet unknown reliability.

In this report a review of four of the methods currently available for the determination of optical parameters is presented. Mixtures of scattering and absorbing particles with known optical parameters (phantom) were used. The methods under investigation are (1) a single or (2) a double integrating sphere: measurement of diffuse reflection and transmission from a sample in either, in combination with collimated transmission through the sample. (3) Light distribution measurements in a Reservoir with Phantom medium and (4) angular dependent transmission through a plane paralel medium with the Goniometer. Light destributions are described by the equation of radiative transfer. The single and double integrating sphere measurement coefficients show good agreement with the exact values for absorption coefficients greater than 0.01 mm^{-1} but not for the scattering coefficient and scattering anisotropy factor, most likely due to problems in the collimated transmission measurements. The space irradiance in the Reservoir with phantom is measured with an isotropic detector and compared with computer calculations from a program by Scott Prahl of the University of Texas at Austin, U.S.A., employing curve fitting to establish the optical parameters. Computer calculations deviate expecially for small beam diameters from experimentally obtained isodose curves. This can be explained by the fact that the diffusion theory is probably no longer valid. This method involves a large volume of material and several combinations of optical parameters may give the same light distribution. The goniometer measures angular dependent transmission through a slab of a turbid medium. Computer simulation by Pascal Storchi of the Rotterdam Radio Therapeutic Institute, Rotterdam, The Netherlands is used to interpret experimental results by curve fitting. The experimentally obtained angular distribution curves deviate from calculated curves probably caused by insufficient scattering events. This will result in not perfectly diffuse light what is necessary for the diffusion approximation.

0. Introduction.

In the continuous search for more efficient and less straining methods for cancer treatment,a new therapy, the Photodynamic therapy (P.D.T.) has recently been introduced.
P.D.T. is based on a photochemical mechanism, and works as follows [53].
The elementary principles for this new therapy date from the begining of this century when a substance was discovered which shows fluorescent activity [39], also when present in living tissue.
Being injected into a living animal affected by cancer, the substance hematoporpherin derivate (HpD) [47] will selectively be retained by cancer cells. After irradiating the tissue surface with light, pronounced fluorescence will show [31] at places where tumor growth is concentrated, when the tumor is close to the surface. Furthermore in the early seventies the healing properties of the photosensitiser on tumors was being investigated for the first time [7].
Hematoporpherin derivative retained in live cells irradiated with visible light induces a photochemical reaction with a toxic product, singlet oxigen when the applied light-dose exceeds a treshold value. The affected cells will die [3].
Due to the relatively small penetration depth of light in tissue the treatment will only be suitable for dealing with superficial cancer [60].

In order to know and predict tissue damage as a result of photo-dynamic therapy, the light-distribution in tissue will have to be known [30].
This knowledge can be obtained from light distribution theory with abundant data (if available) on optical parameters of different kinds of tissue.

The propagation of light in turbid material depends on a variety of factors [9]. The transmission, absorption, reflection, scattering angular distribution and polarisation depend for example on the density of particles, their shape and size relative to the wavelength, their dielectric constant and the index of refraction of the particles and of the medium.

The main approach in light distribution theory is: the equation of radiative transfer [6] [19].

This equation is an integro-differential equation, which uses the absorption coefficient α and scattering coefficient σ and in the diffusion approximation also the so called scattering anisotropic factor (g) that indicates the scattering pattern to describe light distribution.
So far very little is known about the optical parameters of tissues [15]. Even the available methods to determine optical properties have only been developed recently. As yet no suitable standard to verify the results has been found [55].
In this report the following four methods to determine optical parameters will be discussed: (1) Single Integrating Sphere; (2) Double Integrating Sphere; (3) Reservoir with Phantom Medium and (4) Goniometer.
The optical parameters of a suggested standard medium (phantom) and of several organs are being presented to get a better view on the reliability of the optical parameters obtained from the various methods. The wavelength chosen in this report is 632.8 nm from a Helium Neon laser. The optical parameters of tissues at this wavelength are important in view of clinical photodynamic therapy occuring at 630 nm [2] [22].

The data have been acquired in a research project for the Sint Joseph Hospital in Eindhoven, The Netherlands, under supervision of Dr. M.J.C. van Gemert as a graduation project for the University of Technology Eindhoven, Eindhoven, The Netherlands, under supervision of Prof. Dr. J.A. Poulis.
Experiments were carried out at The University of Texas at Austin, Austin, Texas, U.S.A.; the Daniel Den Hoed Clinic, Rotterdam, The Netherlands, and the Sint Joseph Hospital, Eindhoven, The Netherlands.

1. Theory.

1.1. Introduction.

The general equation for photon transport in scattering and absorbing media is the Radiative Transfer Equation [6] [25], which can be analytically solved in only a few cases with well defined boundary conditions and scattering properties.
Steady state light transport in turbid media can be calculated for a limited number of cases, and than only with extensive mathematical methods.

Numerically any problem can be tackled, for example with the Monte Carlo method [12], that follows one photon on its path through the medium. Numerical analysis will
not be discussed in this paper. Also polarisation will not be taken into account.
In all cases discussed in this report (that is at 630 nm wavelength) [61] scattering dominates over absorption in tissue. In that case the equation of radiative transfer can be treated in the so called diffusion approximation. The optical properties are: α = absorption coefficient (mm^{-1}); σ = scattering coefficient and g = expectation value of the cosine of the angle of scattered photons relative to the incoming beam.

1.2. Diffuse approximation.

The equation of radiative transfer is outlined in the appendix. The diffusion approximation will also be discussed here briefly. In case of cylinder symmetry and diffuse illumination of a slab of medium the equation of radiative transfer is given by Ishimaru [25] (see also eq. A28 of the appendix).

$$\mu \frac{\partial I_d(z,\mu)}{\partial z} = -(\alpha+\sigma) I_d(z,\mu) + \int_{-1}^{+1} I_d(z,\mu') P(\mu,\mu') d\mu' \qquad (1)$$

$I_d(z,\mu)$ is the radiance at depth z; $\mu = \cos\Theta$, Θ is the angle with the positive z-direction.

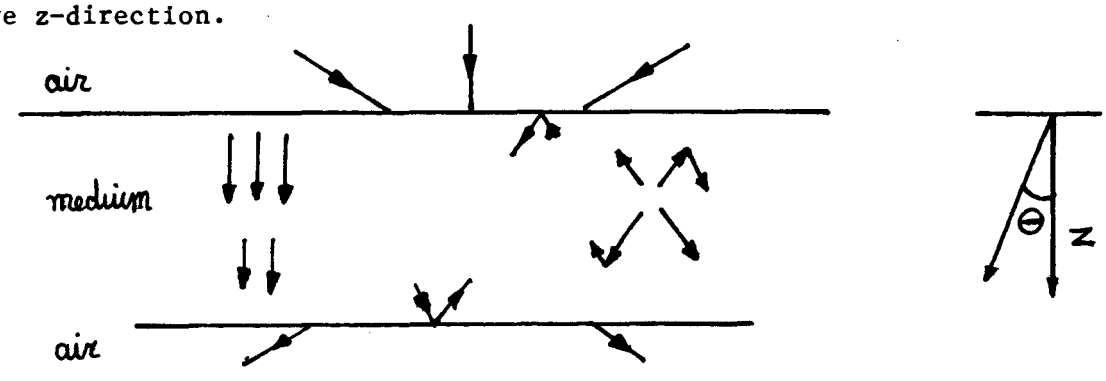

fig. 1 Light propagation in a plane parallel turbid medium.

$P(\mu,\mu')$ = phase function: which defines the problability of scattering from μ to μ'.
We can expand $P(\mu,\mu')$ in a series of Legendre polynomals [76], as descibed in equations A30 to A39 of the appendix.

In the diffusion approximation we only use the first two terms [14] [17]:

$$\frac{d}{dz}\int_{-1}^{+1} I_d(z,\mu)d\mu = -\alpha\int_{-1}^{+1} I_d(z,\mu)d\mu \tag{2}$$

$$\frac{d}{dz}\int_{-1}^{+1} \mu^2 I_d(z,\mu)d = -(\alpha+\sigma)(1-w_1)\int_{-1}^{+1}\mu I_d(z,\mu)d\mu \tag{3}$$

Where:

$$w_1 = \tfrac{1}{2}\int P(\mu,\mu')\mu d\mu' \tag{4}$$

and

$$w_o = \tfrac{1}{2}\int P(\mu,\mu')d\mu' = \frac{\sigma}{\alpha+\sigma} \tag{5}$$

w_o is called the albedo for single scattering.

Next we introduce the expectation value for the cosine of scattering angle:

$$g = \frac{\frac{1}{2}\int_{-1}^{1} P(\mu,\mu')\mu d\mu}{\frac{1}{2}\int_{-1}^{1} P(\mu,\mu')d\mu} = \frac{w_1}{w_o} \tag{6}$$

In the diffusion approximation the radiance $I_d(z,\mu)$ is described by an isotropic part: $U_d(z)$ and a slightly anisotropic part: $F_d(z)$.

$$I_d(z,\mu) = U_d(z) + \frac{3}{4\pi}F_d(z)\mu \tag{7}$$

Where $U_d(z) = \int_{-1}^{1} I_d(z,\mu)d\mu$

$$F_d(z) = \int_{-1}^{1} I_d(z,\mu)\mu d\mu$$

Next we introduce the forward and backward flux as in equations A40 and A41

$$F_{d+}(z) = 2\pi\int_{0}^{1} I_d(z,\mu)d\mu = 2\pi\{\frac{1}{2}U_d(z) + \frac{1}{3}F_d(z)\} \tag{8}$$

$$F_{d-}(z) = -2\pi\int_{-1}^{0} I_d(z,\mu)d\mu = 2\pi\{\frac{1}{2}U_d(z) - \frac{1}{3}F_d(z)\} \tag{9}$$

This will finally result in the following (Van Gemert et al) [14] [18]:

$$\frac{dF_{d+}(z)}{dz} = -\{2\alpha + \frac{3}{4}(\alpha+\sigma)(1-w_1) - \alpha\}F_{d+}(z) + \{\frac{3}{4}(\alpha+\sigma)(1-w_1) - \alpha\}F_{d-}(z) \tag{10}$$

$$-\frac{dF_{d-}(z)}{dz} = -\{2\alpha + \frac{3}{4}(\alpha+\sigma)(1-w_1) - \alpha\}F_{d-}(z) + \{\frac{3}{4}(\alpha+\sigma)(1-w_1) - \alpha\}F_{d+}(z) \tag{11}$$

1.3 Theory of the Integrating sphere.

The integrating sphere is a means of creating diffuse light without much loss of light [10].

A light beam will be allowed to penetrate into the sphere, where the narrow beam is spread out over the surface of the sphere resulting in a lower surface radiance but as a result of the highly reflective coating [38] on the inside of the sphere multiple reflections will occur and give an increase in radiance [29].

A laser beam is incident on a piece of frosted glass G used to create diffuse light in order to assure complete homogeneous illumination of the sphere wal. Let F_1 = the amount of diffuse light flux from the piece of frosted glass incident on the sphere wall, m the absolute reflectance of the sphere wall, A = the area of the complete sphere wall and a = the area of the sphere wall lost due to holes.
Let $1 - a/A = \beta$, the fractional part of the remaining area of the sphere.

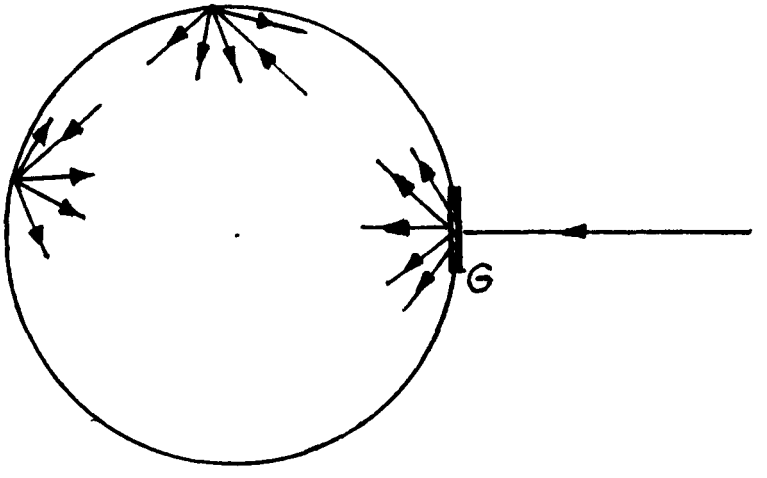

fig. 2 Light intensification from multiple reflections at the sphere wall.

After the first reflection of the incoming flux the radiance N_o of the sphere wall is given by

$$N_o = \frac{F_1 m}{\beta A} \tag{12}$$

And from multiple reflections from the remaining sphere wall this will result in the following expression for the total radiance: N of the sphere wall (Miller) [45]:

$$N = \frac{F_1 m}{\beta A(1-\beta m)} \tag{13}$$

1.3.1 Reflectance of the sphere wall

In order to establish the absolute reflectance of the sphere wall needed for corrections for a non perfect reflecting surface (perfect reflectance m = 1) the following procedure must than be followed. A sphere of radius R is provided with three holes: one for illumination and one for viewing the interior of the sphere and a third hole designed as test aperture.

let c' = spherical area of test aperture

c'' = plane area of test aperture

c_1 = sum of areas of observing and illuminating aperture (because the dimension of these two apertures are kept small the plane area is approximately equal to the spherical area).

let a = $4\pi R^2 - c' - c_1$

m = total diffuse reflection of the sphere surface and standard plate

b_o = mean brightness of sphere wall for reflected light only, test aperture uncovered.

b = dito, test aperture covered with standard plate

(the apertures represented by c_1 are assumed to have zero reflection.

This leads to the following equation (Preston) [51] in the two situations where

1. the test aperture is uncovered

$$b_0 = \frac{m^2 F_0 \{a + c' m(1-c_1)\}/4\pi R^2}{\pi\{(1-m)(a+c''m-c'c_1 m/4\pi R^2)+(c_1 m/4\pi R^2)(mc''+4\pi R^2-c')\}} \tag{14}$$

2. test aperture covered with standard plate

$$b=\frac{m^2F_0a/4\pi R^2}{\pi\{m(c''+c_1-2c'c_1/4\pi R^2)+a(1-m)\}} \qquad (15)$$

The ratio b/b_0 is measured and with the constants c', c'' and c_1, the total diffuse reflection factor m can be obtained.

1.4 Theory for measurements with Single and Double integrating sphere.

For the single and double integrating sphere measurements the transport equation of radiative transfer needs to be solved for an infinite wide slab in the diffusion approximation as outlined in the appendix.
The solution for a diffuse illuminated slab is shown in eq. (10) and (11).

A criteria for the solution of a slab in the diffusion approximation is diffuse illumination of the slab. As a result of a difference in index of refraction (n) of air and sample there will be a critical angle of reflection. This means that a cone of light will enter the sample and light will be trapped inside the sample by total reflection.

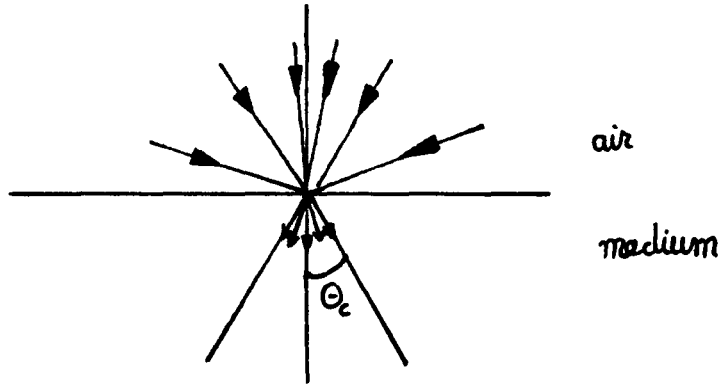

fig. 3 Critical angle θ_c of refraction as a result of a missmatch in index of refraction.

The medium will mainly be water, or for tissue containing much water and the index of refraction of the medium will be n = 1.33. This will result in a critical angle of 49^o. The best way of solving this boundary value problem is by placing the sample in an environment of matching index of refraction. This is not always possible. However, the following was done to imitate index matching. Two glass halfspheres n = 1.5, radius r were placed on either side of a plane parallel medium with the flat side facing the medium (fig. 4).

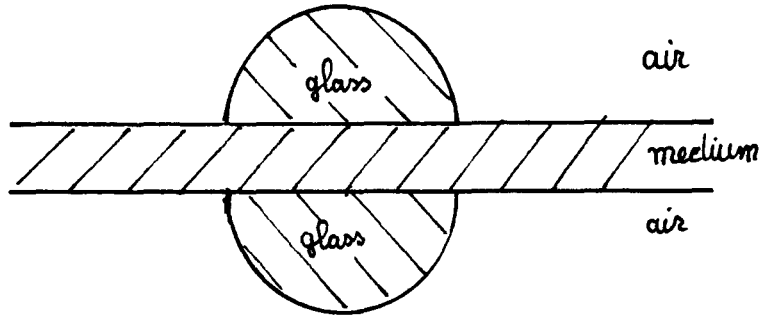

fig. 4 Plane parallel medium with two glass half spheres.

At the glass-air interface however, there is again the problem of critical angle. This will result in an area: A, smaller than the flat surface area that will allow undisturbed passage of light rays from the sample into air, through the glass hemisphere. This can be seen from the following picture (fig. 5):

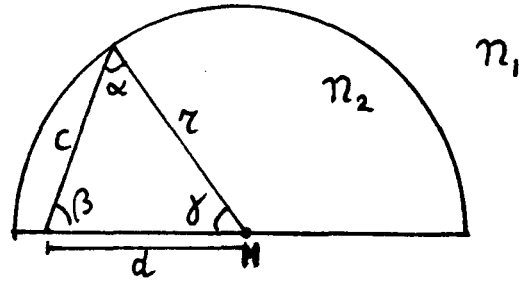

fig. 5 Area under glass hemisphere with " index matching".
α, β, γ angles of a triangle; **d,c,r** *legs of the triangle*
n_1= refractive index of air, n_2= refracttive index of glass.

$$\cos\alpha = \frac{r - d\cos\gamma}{c} \qquad 0^\circ \leq \gamma \leq 90^\circ \tag{16}$$

$$c = \sqrt{d^2 + r^2 - 2dr\cos\gamma} \tag{17}$$

is maximal for $d = R\cos\gamma$

$\cos\gamma$ is maximal for $\sin\alpha$ maximal.

$\sin_{max}\alpha$ is fixed by the critical angle for glass to air and

$$\sin\alpha_{max} = \frac{n_1}{n_2} = \frac{1}{1.5} = \frac{2}{3}$$

The maximum value for $\cos\gamma$ is obtained for $\beta = 90^\circ$ given

$$\cos\gamma_{max} = \sin\alpha_{max} = \frac{2}{3} \tag{18}$$

This will result in an area A with radius d, $d = \frac{2}{3} R$

We now return to the diffusion approximation for a slab with diffuse illumination.

Writing eqs. (10) and (11) as

$$\frac{dF_{d+}(z)}{dz} = -(K+S)F_{d+}(z) + SF_{d-}(z) \tag{19}$$

$$\frac{dF_{d-}(z)}{dz} = -(K+S)F_{d-}(z) + SF_{d+}(z) \tag{20}$$

where K = the absorption coefficient and

S = the scattering coefficient.

Solving these equations for a diffuse light source at the surface z=0 and no light coming from the surface at z = d (black backing), this means no reflection at the medium interfaces with the following boundary condition

$$F_d+(0) = I_o \tag{21}$$

$$F_d-(d) = 0 \tag{22}$$

leads to the following solutions: [Kubelka] [36] [37]

$$F_d+(z) = c_1 e^{bSz} + c_2 e^{-bSz} \tag{23}$$

$$F_d-(z) = (a+b)c_1 e^{bSz} + (a-b)c_2 e^{-bSz} \tag{24}$$

where $$a = \frac{S+K}{S} \tag{25}$$

$$b = \sqrt{a^2-1} \tag{26}$$

with the boundary conditions (21) and (22) we get

$$c_1 = \frac{I_o}{1+\frac{a+b}{a-b}} e^{-2bSd} \tag{27}$$

$$c_2 = \frac{I_o}{1+\frac{b-a}{a+b}} e^{2bSd} \tag{28}$$

This allows the solution to be written as

$$F_d^+(z) = I_o \frac{a \sinh bSz + b \cosh bSz}{a \sinh bSd + b \cosh bSd} \tag{29}$$

$$F_d^-(z) = I_o \frac{\sinh bSz}{a \sinh bSd + b \cosh bSd} \tag{30}$$

This yields for the reflection and transmission coefficient

$$R = \frac{F_{d-}(0)}{I_0} = \frac{\sinh bSd}{a \sinh bSd + b \cosh bSd} \tag{31}$$

from eq. (30) the reflectivity of an infinitely thick medium can be obtained using:

$$R_\infty = \lim_{z-\infty} R \quad \text{and will yield (27)} \quad R_\infty = a-b \tag{32}$$

$$T = \frac{F_{d+}(d)}{I_0} = \frac{b}{a \sinh bSd + b \cosh bSd} \tag{33}$$

solving S and a from eq. (31) and (33) leads to

$$S = \frac{1}{bd} \ell n \left\{ \frac{\frac{b}{T} + \sqrt{\left(\frac{b}{T}\right)^2 + 1}}{a+b} \right\} \tag{34}$$

and $$a = \frac{1+R^2-T^2}{2R} \tag{35}$$

Comparing the coefficient [13],[16],[33] from eq.(10) and(11), and eq. (19) and (20) will give α and $\sigma(1-g)$ as a function of R and T [17]. If next the total collimated transmission is determinened, the total attenuation coefficient
$(\alpha+\sigma)$ will follow from Beer's law [4] and the individual values of α, σ and g can be calculated.
Reflection and transmission measurements are done with the integrating spheres as decribed in paragraphs 2.3 and 2.4.
The relection coefficient R will follow from the following individual measurements [63]: reflection at a perfectly reflecting plate at the sample hole: R_{100}, with a correction for a not perfectly reflecting surface. Reflection with the sample hole uncovered, so called black hole reflection: R_o. And finally reflection from the sample on the sample hole: Rs.

$$R = \frac{R_s - R_0}{R_{100}\frac{100}{m} - R_0} \tag{36}$$

Where m is the reflection factor of the diffuse reflecting coating of the integrating sphere.
The same procedure is used for transmission with the exception that care is taken to assure that T_o (0 % transmission) to be zero. This leads to:

$$T = T_s/T_{100} \tag{37}$$

where T_s = transmission through the sample and T_{100} = 100 % transmission.This will give the individual values of α, σ and g according to the following equations [5] [17]:

$$K = (a-1).S \tag{38}$$

$$\alpha = K/2 \tag{39}$$

$$q = \alpha+\sigma = \frac{1}{d}\ln\{\frac{I_c(0)}{I_c(d)}\} \quad ; \text{ d= thickness of the sample} \tag{40}$$

$I_c(o)$= the radiance of the incident collimated beam,
$I_c(d)$= the unscattered transmitted beam through the sample of thickness d.

$$\sigma = q-\alpha \tag{41}$$

$$g = \frac{1-\frac{4(S+\alpha)}{3q}}{w_o} \quad ; \quad w_o = \frac{\sigma}{\alpha+\sigma} \tag{42}$$

1.5 Theory for Reservoir with phantom medium.

For a (large) phantom with depth d with a collimated beam of light incident normally upon the air-liquid interface, two situations can be examined. The first case is a plane wave which is equivalent to a beam of infinite width. The second case is a collimated beam of finite width.

Starting from the diffusion equation (Ishimaru) [25], see also eq. A25 .

$$\nabla^2 U_d(r)-\kappa_d^2 U_d(r)= -\sigma\sigma_{tr}U_c(r)- \frac{3}{4\pi}\sigma_{tr}E(r)+ \frac{3}{4\pi}\nabla. \int\varepsilon_{ri}(r,s)d\omega+ \frac{3}{4\pi}\nabla. \int\varepsilon(r,s)sd\omega \tag{43}$$

In the case of an infinite wide beam $F_o(r)$ becomes constant F_o, leading to the following diffusion equation:

$$\frac{\partial^2}{\partial z^2}U_d(z)-\kappa_d^2 U_d(z)= -Q_0\exp(-qz) \tag{44}$$

where $Q_0= \{3\sigma\sigma_{tr}+3\sigma qg\}\frac{F_0}{4\pi}$

The general solution of eq. (43) consists of a particular solution

$$U_{dp}(z) = A\exp(-qz) \qquad A= -\frac{Q_0}{q^2-\kappa_d^2} \tag{45}$$

and a complementary solution

$$U_{dc}(z) = C_1\exp(\kappa_d z) + C_2\exp(-\kappa_d z) \tag{46}$$

Where C_1 and C_2 are constant coefficients from the solution

A case of special interest is when the medium is of semi-infinite thickness, this will let C_1 go to zero (Ishimaru) [25] and leaves us the following solution:

$$U_d(z) = A\exp(-qz) + C_2\exp(-\kappa_d z) \tag{47}$$

At greater depths equation (47) will be governed by the latter part of the equation giving a tool to (establish) the so called effective attenuation coefficient K_d to describe the light distribution at depths greater than three or four free optical path lenghts.
The effective attenuation coefficient κ_d is given by

$$\kappa_d^2 = 3\alpha\sigma_{tr} \tag{48}$$

where σ_{tr} = the transport coefficient

The solution for a collimated beam of finite width is the second case of interest. A general solution of eq. (43) is described by Ishimaru and Chandrasekhar [25] [6].
A computer program based on the diffusion equation solution by Groenhuis et al. [20], developed by Scott Prahl of the University of Texas at Austin [50] gives an analytical solution.

1.5.1 LIGHT INTENSIFICATION BY MULTIPLE SCATTERING

When a plane wave is incident on a semi-infinite medium of scattering particles, the space irradiance directly below the surface can be several times the incident space irradiance, [55]. This can be explaned qualitatively by multiple reflections; as follows
If we consider a half infinite phantom with a plane wave incident on the medium, as outlined in figure 6.

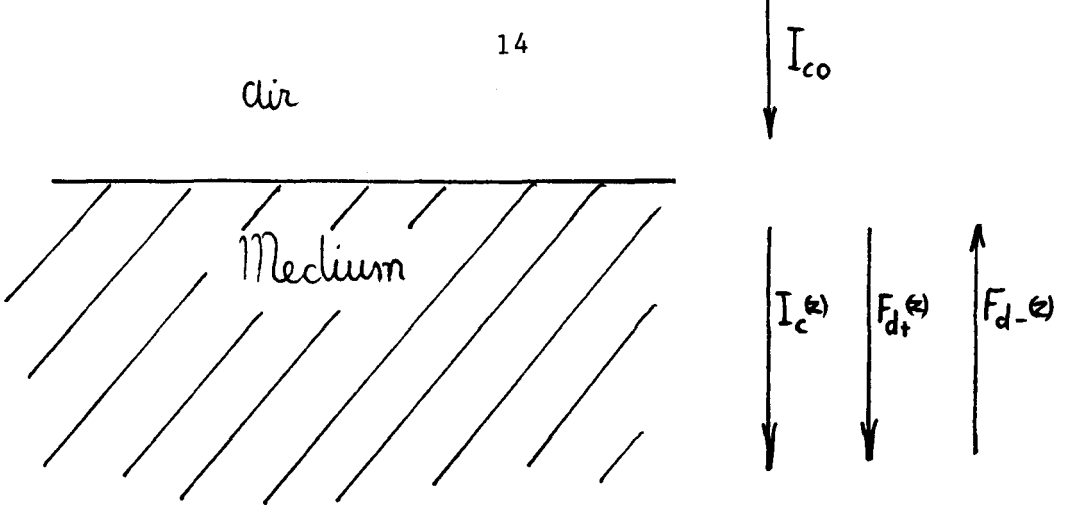

fig. 6 Light flux diagram.

$I_{co}(z)$ = incident beam radiance.
$I_c(z)$ = radiance of the reduced collimated beam
$F_d+(z)$ = forward flux of diffuse light
$F_d-(z)$ = backward flux of diffuse light.

At the phantom-air interface the reflection coefficient r_i for diffuse light is goverend by the critical angle and is given by $r = r_{id}$ (Kottler) [34], r_{id} = the internal diffuse reflection coefficient.

For a scattering medium the half space is replaced by a thin surface layer, of only a couple of free optical path lengths thick, and a second layer [52]. (fig. 7).

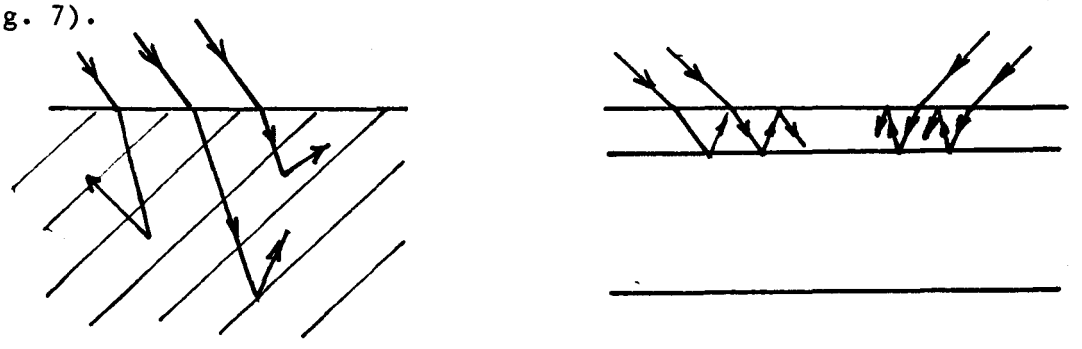

fig. 7 Light intensification by multiple reflections in a plane parallel layer.

The reflection coefficient at the second interface is given by the reflection factor for an half infinite medium as given by equation (Kubelka) [36] $r_2 = R_\infty$

The relative radiant flux density = $\frac{I_{internal}}{I_{co}}$

(where I internal = radiant flux density inside the medium just below the surface), in the first layer result from multiple reflection between the two interfaces.

$= I_c(z) + 2[F_{d+}(z) + F_{d-}(z)]$ (Kottler) [35] can be calculated from multiple reflections [46].

$$\frac{I_{internal}}{I_{co}} = 1+2\{\sum_1^{\infty} r_2^n r_1^n + \sum_1^{\infty} r_2^n r_1^{n-1}\} = 1+ 2\{\frac{r_2(r_1+1)}{1-r_2r_1}\} \qquad (49)$$

Example: 2% intralipid (10%)
$\sigma = 1.1\ mm^{-1}$; $\alpha = 0.0002\ mm^{-1}$; g = 0.83 yields
$r_2 = R_\infty = 0.927$; $r_1 = r_{id} = 0.596$ for diffuse light at the water-air interface [34], and with equation 49:

$$\frac{I_{intern}}{I_o} = 7.6$$

1.6 Theory for Goniometer.

With the goniometer the angular distribution of light from a collimated beam through a plane parallel medium is determined. A comparison is amde with a computer model based on the equation of radiative transfer with calculations for selected values of α, σ and g. The computer model was designed by Pascal Storchi of the Daniel den Hoed Clinic, Rotterdam, The Netherlands. The complete theory will not be discussed here but is described by Chandrasekhar [6].

2. Materials and methods.

2.1. Introduction.

There are several methods available to determine the optical properties; absorption coefficient: α, scattering coefficient: σ and scattering anisotropy factor: g.

Every method uses the solution to the transport equation, with different initial values and boundary conditions.
The difference in approach depends on whether collimated or diffuse incident light is used and whether the indices of refraction of the subsequent layers match or not [33].
The four methods under investigation are: (1) Single Integrating Sphere, (2) Double Integraring Sphere, (3) Reservoir with phantom medium and (4) Goniometer.
Single and Double Integrating sphere measurements are based on the determination of the diffuse reflection and transmission coefficient from a plane parallel medium in combination with the total collimated attenuation [11] through the sample (see equation (31-42). The Reservoir with phantom is used to measure the light distribution inside a phantom in substitution for tissue. Goniometer experiments give angular dependant transmission through a plane parallel medium.
To compare the afforementioned 4 methods, a standard medium has been defined and used. The medium under investigation, called a phantom, is a mixture of a solution of predominantly scattering particles and a solution of exclusively absorbing particles.

The scattering medium is either intralipid (10%) or styrene butadiene. Intralipid (10%) is a white fatty substance used for intraveneous nutrition for patients in the hospital and has a g-value of approximately 0.83 [44],[49],[58] and is available in a standard 10% solution. Styrene butadiene is an artificially composed chemical consisting of small white spheres of 0.2 μm diameter and g equals roughly 0.38 [24],[32],[58] at 632.8 nm.
The absorbing medium is indian ink or colouring for food (blue).

By diluting the solutions we can adjust the optical parameters of each medium. Mixing the scattering and absorbing substance with known proportion will give any desired optical composition of alfa an sigma, only the g-value can not be varied. The choise whether intralipid or styrene butadiene is used as scatterer will dictate the g-value.

For integrating sphere measurements the scattering and absorbing particles have to be suspended in a gell. By adding clear agar (3 grams per 100 ml) to the solution and adding heat until it starts to boil, a solid substance with presumably the same optical properties as the liquid is obtained.

The thickness of the sample is important. The sample must be at least three free optical path lengths thick to insure diffuse light inside the medium [7], to satisfy the diffusion approximation. This criteria is imposed by the fact that in most cases at the air-medium interface the angular distribution of light in response to diffuse incidence will be limited inside the sample by the critical angle because of mismatch in index of refraction [4].

For the reservoir and the goniometer, a wide parallel beam is obtained from a broad band light source with a 630 nm, bandwidth 10 nm, and a lense with aperture.
All experiments have been done at the same wavelenght to eliminate wavelength dependance of the optical parameters.
The detected light was monitored with a lock-in amplifier to eliminate ambient light.

2.2 Integrating sphere.

First the concept of the so called integrating sphere will be discussed.
The mechanisme of the integrating sphere was described for the first time by Ulbricht (1928) and is also refered to as "Ulbricht-sphere" [23] (fig.2).
A sphere is coated on the inside with a highly diffuse-reflective paint ($BaSO_4$, m = 0,95) [1],[38]. The reflection factor (m) of the white coating of the sphere can be established by reflection measurements [45] in the sphere according to equation (14 and 15). The diffuse reflecting paint reflects light according to Lambert's law ($I(\theta) = I_o \cos\theta$) [4]. Through a hole in the wall light is being conducted into the sphere. Inside the sphere the light will reflect on the white wall, and the wall of the sphere will be homogeneously diffuse illuminated. Because of multiple reflections there will also be an increase in radiance [27].
When another hole is made in the sphere, it can be used as a diffuse light source. Or it can be used as a geometry-independant light detector [63].

The holes used for conducting light in or out the sphere for light delivery or detection must be kept as small as possible to avoid effecting the efficiency of the integrating sphere.
The holes in the sphere must be positioned in such a way that, with the viewing-angel of the specific hole, one hole can not detect light coming

directly from another hole. If this situation does exist it must be prevented by shealding one of the holes with a so called baffle.
This does not apply for the single integrating sphere because the two detector holes are facing each other.

The sample holes in the sphere for measuring transmittance and reflectance must be about 1% of the total surface area of the the sphere to detect up to 10% change in radiance for reflection measurements between a black hole or a white standard coverplate (equations 14 and 15) [51].
The holes must not be to large so that the integrating properties will not be affected. A total of 1.65% of surface area with a reflection factor of zero will result in a decrease of 25% in surface radiance in the sphere, compared to the complete integrating sphere (equation 13) [45].
The coating of the interior of the sphere must have a high reflection factor, because the relative change in reflection by removing a portion of the wall of the sphere and replacing it with a surface with a lower reflaction factor will dictate the accuracy of the measurements.

2.3 Single integrating sphere.

A scematic view is shown in figure 8. Dimensions: sphere diameter: 110mm, sample hole diameter: 12mm, illuminating hole: 8mm. This sphere was made by Ruud Verdaasdonk (traineeship, St. Joseph Hospital, 1984) [59].
A sample is placed on top of the sphere, position A. Light falls on a piece of frosted glass: G, in a small hole in the sphere at ninety degrees with respect to the detection holes. The diffuse transmittance is measured directly with a detector at the rear of the sample which is placed on the large hole of the sphere, the detector is facing the sample, detector D_1. The relative Transmittance is calculated as described in eq. 33

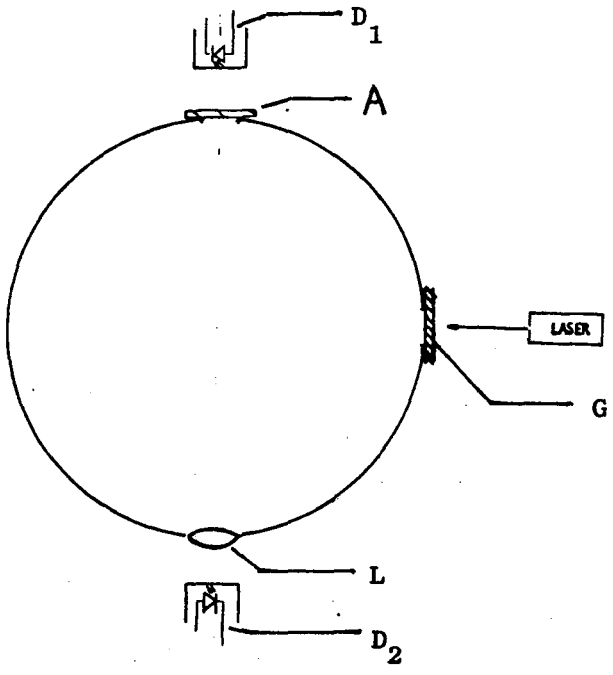

fig. 8 Single intergrating sphere.

For reflection measurements, the detector hole is positioned opposite the sample and a lens (L) focuses the reflected but diffuse light from the sample on a detector, D_2.
By comparing this with reflection from a standard plate in the same position as the sample will give the relative Reflectance, as described in equation 31. In this way the sample size can be kept even smaller than with the double integrating sphere (see below).
A total collimated attenuation by collimated transmission is also required to obtain three sets of equations for the three parameters (see eq. 38,42) Total collimated attenuation is obtained as follows. The sample, of known thickness, is illuminated by collimated light (in most cases a laser beam). The beam is perpendicular to the surface of the sample with an apperture in front of the sample. At approximately 50 cm from the sample, directly in the beam is a light detector with the same apperture. The assumption is made that the decrease in radiance is proportional to the incident radiance (Beer's Law). The experimental set-up for total collimated transmision is shown in fig. 9. A_1 and A_2 are aperture of 2 mm diameter, S is the sample of thickness d, D is a photodiode, x_1 and x_2 are distances that can be varied.

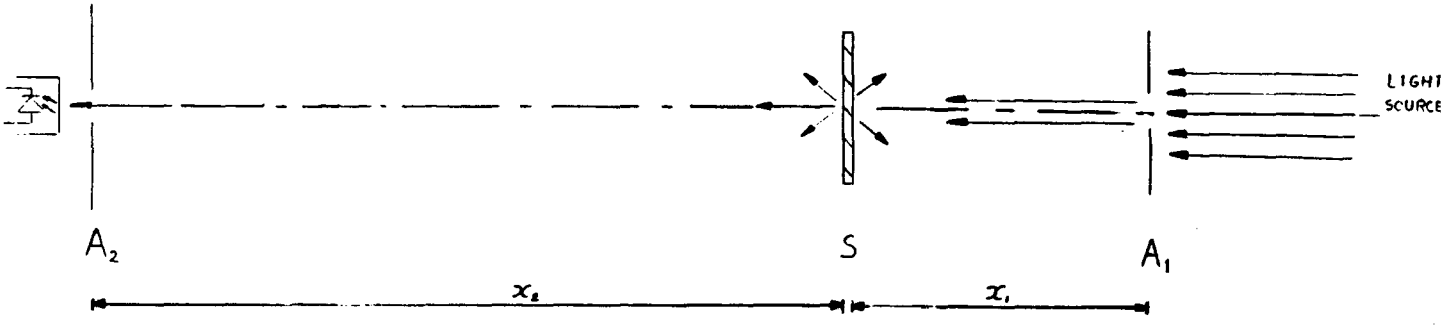

fig. 9 Total collimated transmission.

2.4 Double integrating sphere.

The double integrating sphere is a composition of two integrating spheres linked to eachother by a hole in the two spheres [51]. In this hole a glass hemisphere is placed.
The double integrating sphere is outlined in figure 10. The lower sphere will act as a diffuse light source for the sample placed in position A and the upper sphere will detect the transmitted diffuse light.
A gell with known optical parameters is placed in between the two glass-half spheres in the large hole in the integrating sphere. The flat sides are facing the sample located at position A.
The two spheres are mounted on a platform with three rods to be able to move the spheres in the vertical direction.

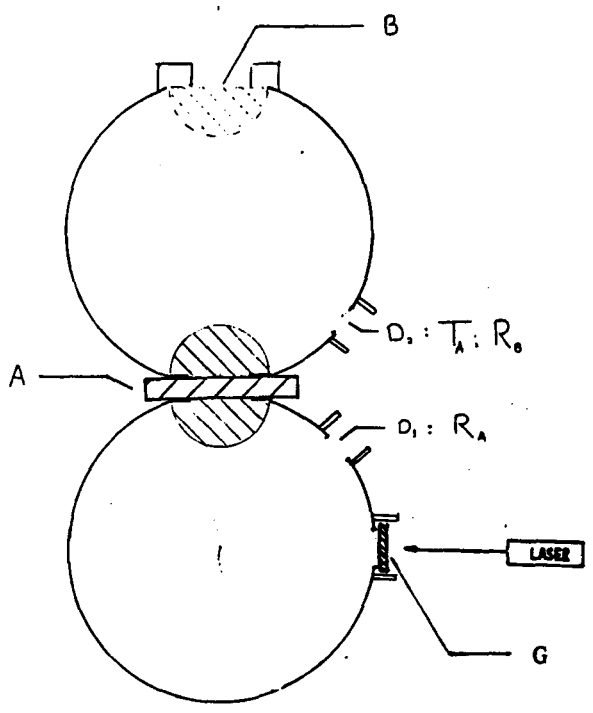

fig. 10 Double integrating sphere

Dimensions: sphere diameter: 80mm for both spheres, diameter glass half sphere: 25mm, effective sample diameter: 16mm, detection holes D_1 and D_2: diameter D_1 and D_2: 8mm, illuminating hole diameter: 10mm. Diffuse light is guided into the first sphere, by laser light incident on a piece of frosted glass (G) present in one of the holes of the sphere.

The sample is shielded from the incoming direct light to assure perfect diffuse illumination of the sample, and diffuse reflection can be measured with a photo diode in this sphere. In the second sphere a light detector detects the transmitted light. Comparing the light intensity in the second sphere with and without sample will give a relative measurement of the radiance. For reflection measurements the sample can be placed on top of a third hole in the second sphere, again with a glass half-sphere as boundary, position B. The standard plate in position B is than replaced by a glass half sphere. The reflected light is measured and compared with the situation where this hole is covered with a disk coated with the same paint as the wall of the sphere.

Combining the diffuse reflection and transmission coefficients and the total attenuaton coefficient, the optical parameters: α, σ and g can be determined within the diffusion approximation for a thin slab (eq. 32-42).

2.5 Reservoir with phantom medium.

A reservoir; cylinder or box, is filled with a medium. The upper surface is an air medium interface, while all other boundaries are preferably white walls to simulate a half infinite space by avoiding reflections from the wall.This is shown scematically in figures 11 and 12.

By placing an aperture (A_1) in front of the light bulb (B), in the focal point of the large positive lens (L), a collimated light beam is produced, see fig. 5.

For the large positive lens a magnifying glass is used with 12 cm diameter and focal lenght of 5cm. To reduce the beam diameter an aperture (A_2) is placed close to the liquid surface, to eliminate interference.

When a filter(F) is placed in between the high power, broad band, light bulb (eg. Xenon lamp) and the aperture, light of selected wavelength will be emitted, preferably 630 nm to comply with the He-Ne laser used for the other experiments.

The diameter of the lens will determine the maximum beam diameter.

The light rays are incident perpendicularly to the air-liquid interface.

The dimensions of the reservoir are large compared to the diameter of the incident beam. The dimensions sould be at least the largest beam diameter plus ten times the free optical-length of the phantom. This is necessary to eliminate reflection from the walls. Box dimensions: 150x150x150mm.

Inside the medium the light distribution is determined. The space irradiance is measured as a function of depth and as a function of radial distance from to the central axis of the beam. The light distibution inside the phantom is measured with a so called isotropic detector. The isotropic detector is a small sphere (radius 0.5 mm) from scattering material that has an allmost uniform sensitivity over all sollid angles, except for the area where the glass fiber is inserted, necessary to conduct the captured light to a photodetector. The isotropic detector was develloped by Hans Marijnissen of the Daniel Den Hoed Clinic in Rotterdam, The Netherlands [7]. The reservoir with isotropic detector is pictured in figure 11. The detector is mounted on a set of two spindles and has two degrees of freedom: axial and radial. The movement in both directions is monitored either with a rular in one experiment, or with a variable resistor in another.

The total collimated attenuation coefficient will be established by on axis radiance gradient measurements with a bare fibre, as shown in figure 12. The fibre's narrow opening-angle is directed towards the incident light beam [7].

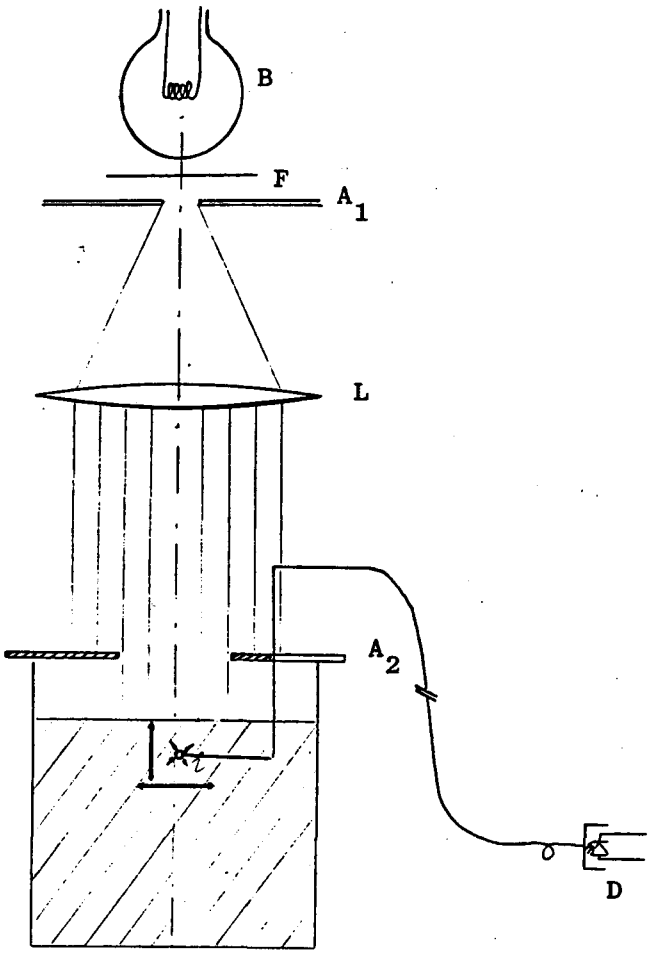

fig. 11 Reservoir with phantom and isotropic detector (i), D *is a photomultiplier.*

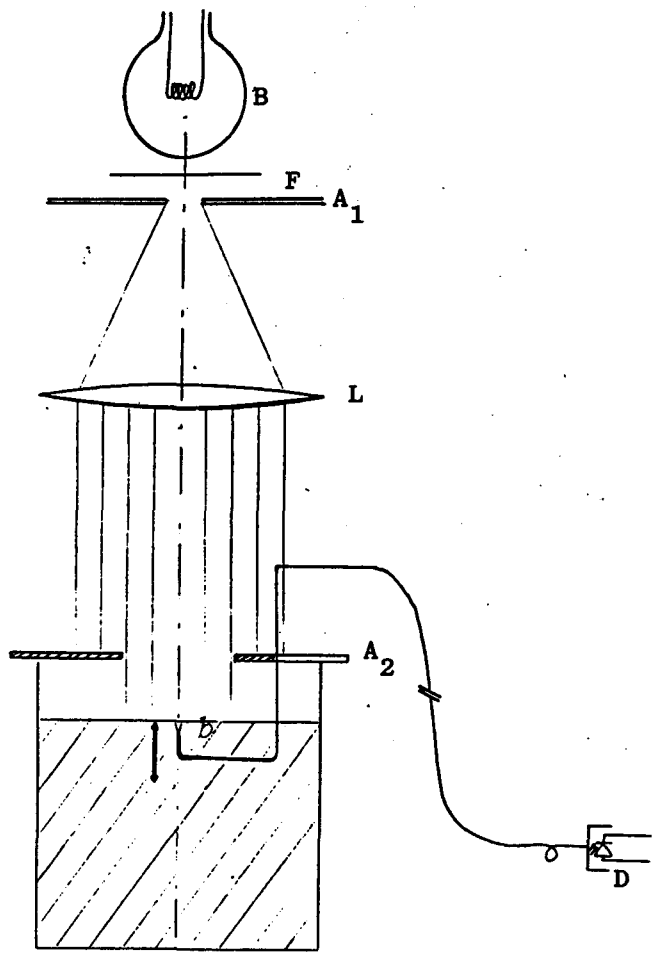

fig. 12 Reservoir with phantom and bare fiber (b), D *is the photomultiplier.*

With known optical properties, the light distibution inside the medium can be calculated and compared to the measured spatial light distribution. This gives information whether the theory is reliable or not [28],[50].
The optical parameters are determined by curve-fitting. A first approximation to the optical parameters is obtained from the previously mentioned methods.

2.6 Goniometer.

In this geometry, a plane parallel sample is placed in a collimated beam of finite diameter, with the plane area perpendicular to the beam.

The sample may be either in air or in water, preferably in a surrounding of matched refractive index. The experimental setup is sketched in fig 13.
The thickness of the sample must be at least three optical free path lengths to ensure necessary for the comparison with diffusion theory.
A glass cuvet will serve as a sample. The cuvet has a cylindrical opening that also serves as aperture, with the wall painted white to suggest an infinite wide medium. The cylinder is 5 or 10 mm long with an inside diameter of 40 mm and is closed on both sides with a glass plate. The cuvet is filled with phantom material and is situated in water. The wall of the cylinder has two small holes to allow replacement of the medium.

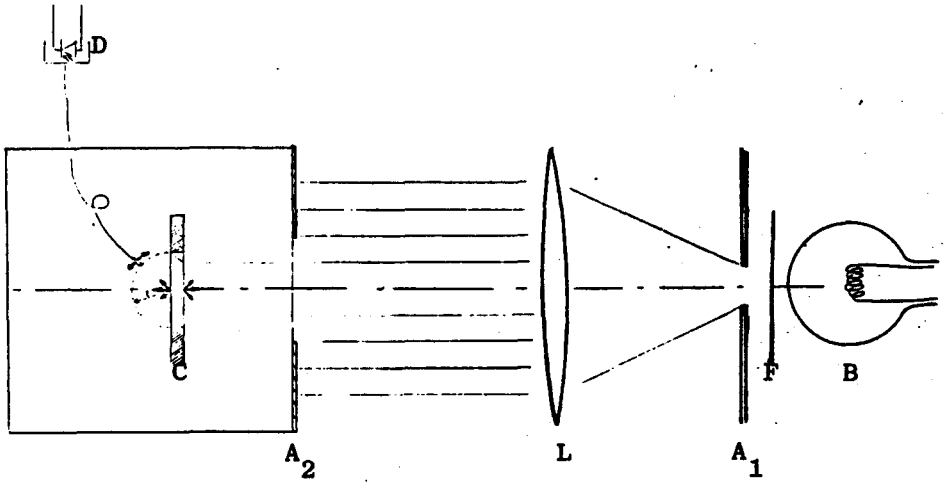

fig. 13 Goniometer. F *is a 630 nm filter,* A_1 *and* A_2 *are apertures,* L *is a lens (f= 5cm) and* C *is the cuvet.*

The glass material of the cuvet does not exactly match the index of refraction of water, but the resemblance seems good enough to assume that total reflections can be neglected.
A fiber with an opening angle (Full Width Half Maximum) of 10 degrees is directed towards the centre of the beam and will guide the light to the photomultiplier. Rotation in the plane perpendicular to the surface of the cuvet at a radius of 20 mm to the centre of the cylinder will give the (light distribution) as a function of the azimuth.

The angle of the detection fiber with the outward normal of the cuvet surface is registered with a variable resistor, that allows an inaccuracy of ± 0.5 degrees.
The scanning radius must be smaller than the size of the sample, but the detecting fibre tip must on the one hand be far enough to detect independent scattering events although on the other hand not too far to maintain angular resolution. In practice a scannig radius of four times the maximum optical free path lenght has been chosen.
These measurements are compared to calculations based on mathematical models for this geometry. By curve-fitting the optical properties can be determined [40].
Another possibility for first order approximations are a number of tables by Van de Hulst. In two of his books the scattered radiance as a function of the scattering angle from thin samples is tabulated for: thickness (in units of free optical path lenghts), albedo (albedo $w_o = \sigma/(\alpha+\sigma)$) and g value

2.7 Sample thickness.

The sample thickness is measured with a micrometer, either directly on the sample or with the sample placed in between two glass-slides for soft media. The samples have not undergone changes in thickness during the measurements due to compression or dehydration in this model.

3. Results.

3.1 Introduction.

Results of the various experiments on phantoms on the determination of the optical parameters are presented in this chapter. The experiments were done at The University of Texas at Austin, Texas, U.S.A., The Rotterdam Radio Therapeutic Institute - Daniel den Hoed Clinic Rotterdam and the St. Joseph Hospital - Eindhoven, The Netherlands.
The results of the sigle and double integrating spheres are presented together in paragraph 3.2., because these two methods appear to be very similar. In paragraph 3.3 the results from measurements in the reservoir with phantom material are presented; first the results from on axis measurements with a

Tabel 1. **Absorption and scattering coefficients of ingredients of phantoms from collimated transmission measurements. with standard deviation.**

CONCENTRATION of scatterers (%)	SCATTERING COEFFICIENT σ (mm^{-1}) of Intralipid (10%) $\sigma = 50 \pm 10\ mm^{-1}$	Styrene butadiene $\sigma = 117 \pm 3\ mm^{-1}$
0.09		0.105 ± 0.003
0.18		0.210 ± 0.006
0.36		0.420 ± 0.012
0.50	0.25 ± 0.05	
0.60	0.3 ± 0.06	
1.0	0.5 ± 0.1	1.17 ± 0.03
1.3		1.52 ± 0.04
2	1.0 ± 0.2	
3	1.5 ± 0.3	
4	2.0 ± 0.4	
5	2.5 ± 0.5	
100	50 ± 10	117 ± 3

CONCENTRATION of absorber (%)	ABSORPTION COEFFICIENT α (mm^{-1}) OF THREE DIFFERENT SOLUTIONS OF INDIAN INK $\alpha_1 = 0.15 \pm 0.02\ mm^{-1}$	$\alpha_2 = 20 \pm 1.0\ mm^{-1}$	$\alpha_3 = 0.45 \pm 0.01\ mm^{-1}$
0.5		0.100±0.005	
0.8		0.160±0.008	
1.0	0.0015±0.0002	0.20±0.01	0.0045±0.0001
2			0.0090±0.0002
10	0.015 ±0.002		0.045 ±0.001
20	0.030 ±0.004		
100	0.15 ±0.02	20 ± 1	0.45 ± 0.01

1% = 10 ml of phantom medium In 1 liter of water.

Intralipid was available in 10% solution.

bare fiber, then the data obtained from on axis measurements with the isotropic detector, and finally the isodose curves comparing measurements with associated computer calculations. In paragraph 3.4 the measurements showing angular dependent transmission curves are compared with computer modelling. The scattering coefficients of pure Intralipid (10%) and pure styrene butadiene are the same throughout all experiments. From reduced collimated light measurements the values are:

intralipid (10%) $\sigma = 50 \pm 10$ mm^{-1} and

styrene butadiene $\sigma = 117 \pm 3$ mm^{-1} .

The absorption coefficient for intralipid (10%) has been established at $\alpha = 0.01$ mm^{-1} as determined by W.M. Star and Hans Marijnissen [55] of the Daniel Den Hoed Clinic in Rotterdam. The optical parameters of the ingredients of the phantom are tabulated in tabel 1. There is still a large standard deviation in the values for α and σ, of the phantoms determined by the various methods.

3.2 Single and double integrating sphere measurements.

Reflection measurments comparing black hole reflection to reflection from a standard plate give a reflection factor of m = 0.93 for the coating of the integrating spheres. In this paragraph the absorption and scattering coefficients and scattering anisotropy factors for gells containing intralipid or styrene butadiene as scatterer in various concentration and food colouring or indian ink as absorber in various concentrations are shown, resulting from collimated and diffuse transmission and diffuse reflection measurements. See equations 33 to 41. The thickness of the samples range from several tenths of a mm to several mm. The results are presented with vertical bars indicating experimental inaccuracy from differential error calculations. Only when the inaccuracy falls below $\pm$ 100% the inaccuracy is indicated by two small vertical arrows. When the inaccuracy exceeds $\pm$ 200% no inaccuracy is indicated.

Figs. 3.2.1-5 show the results for α, σ and g for intralipid with or without absorbing particles. Fig. 3.2.1 and 3.2.2 show the results for experiments performed at Austin. The absorber used in the results of fig.3.2.2 is food colouring (Adam's extract, blue). Fig.3.3.3-5 are data obtained at the St. Joseph Hospital, Eindhoven.

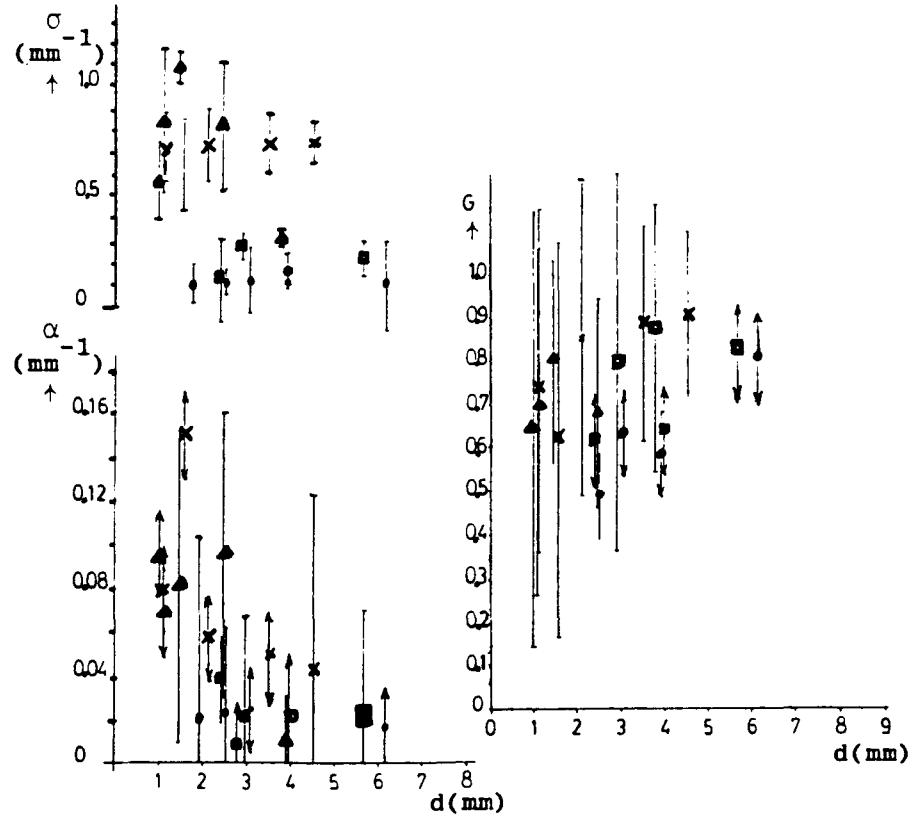

Fig. 3.2.1 α, σ *and g versus thickness (d) of sample Intralipid (10%): 1% • ,2% □ ,4% × ,5% △ ; Double integrating sphere: position B.*

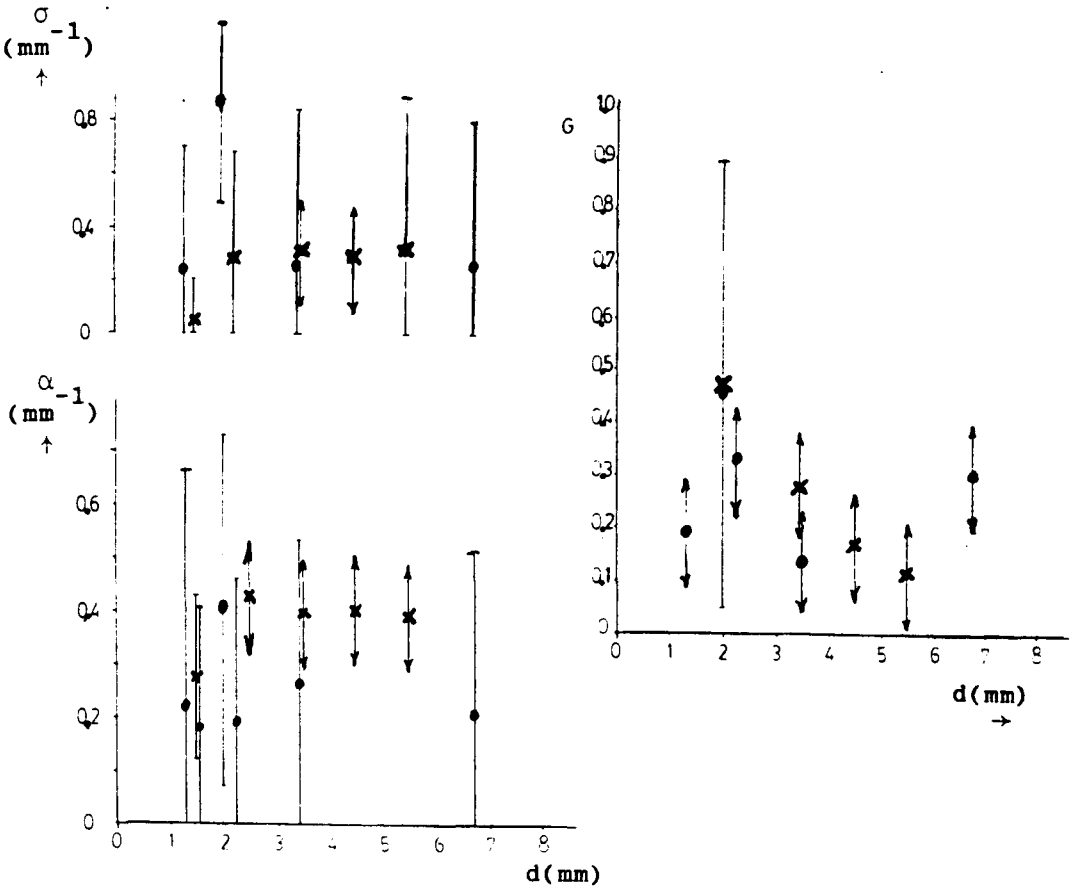

Fig. 3.2.2 α, σ *and g versus thickness (d) of sample Intralipid (10%), 25% • ,50% × absorber; Double integrating sphere: position B.*

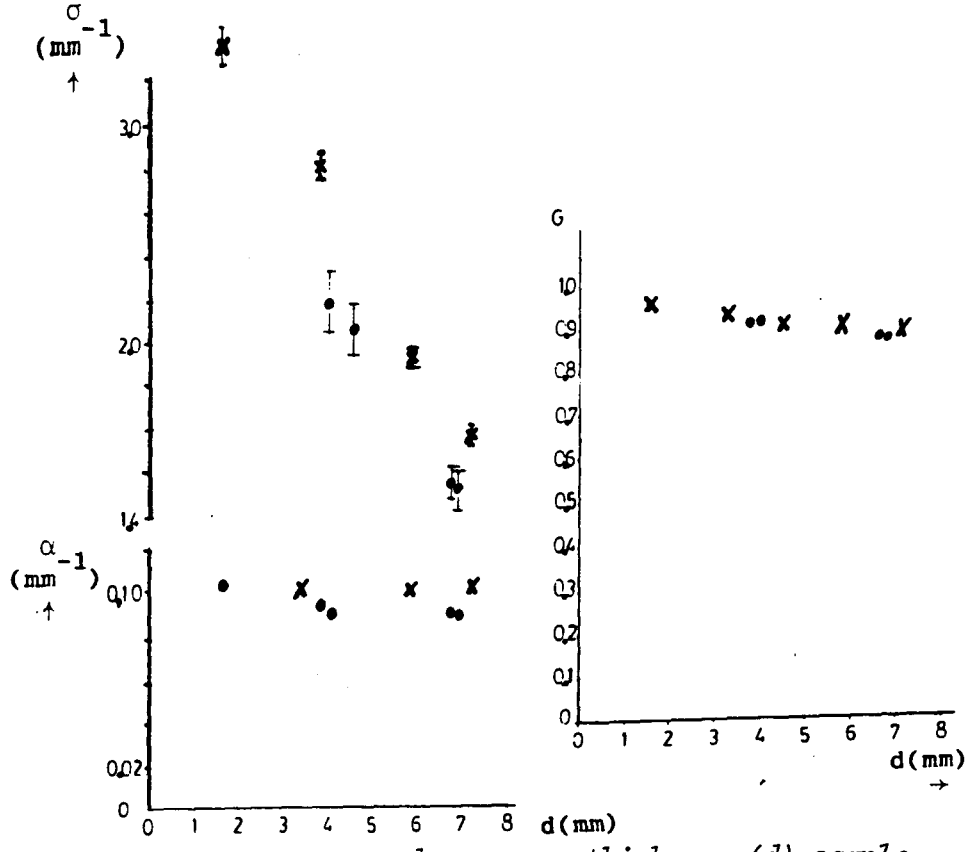

Fig. 3.2.3 α, σ *and g versus thickness (d) sample Intralipid (10%), 1% • ,3% × : 20% India ink. Double integrating sphere: position A.*

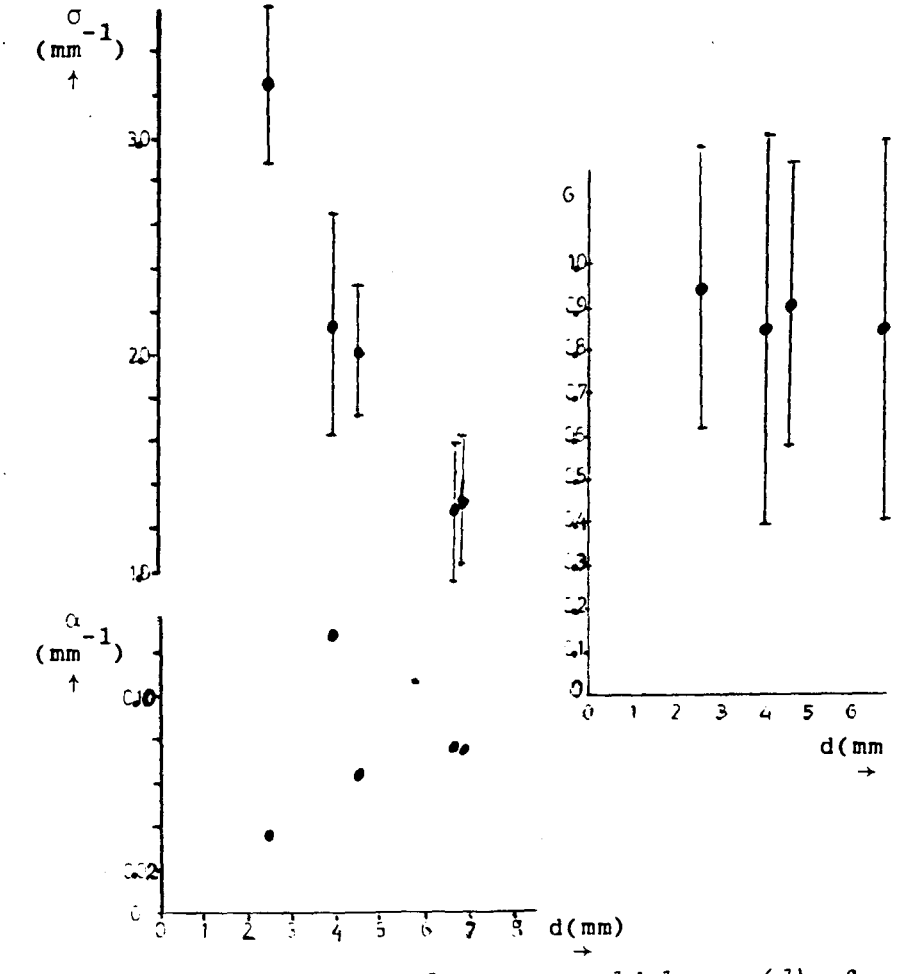

Fig. 3.2.4 α, σ *and g versus thickness (d) of sample Intralipid (10%), 1%; 20% India ink Double integrating sphere: position B.*

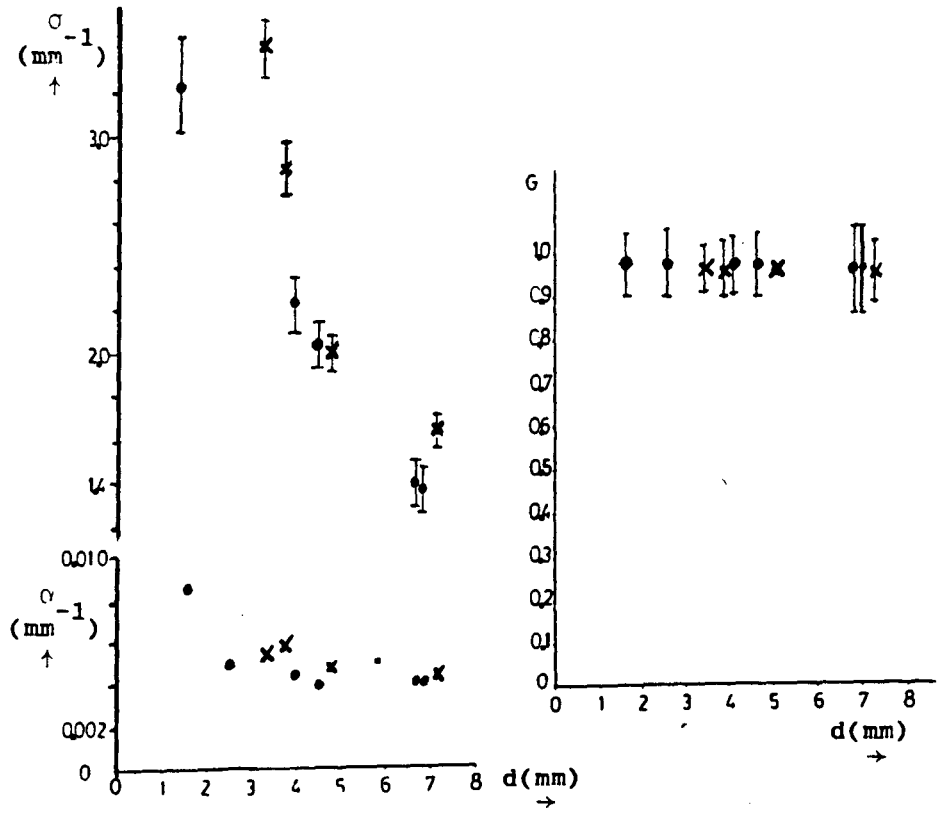

Fig. 3.2.5 α, σ *and g versus thickness (d) of sample*
Intralipid (10%): 1% • , 3% × ; 20% India ink
Single sphere

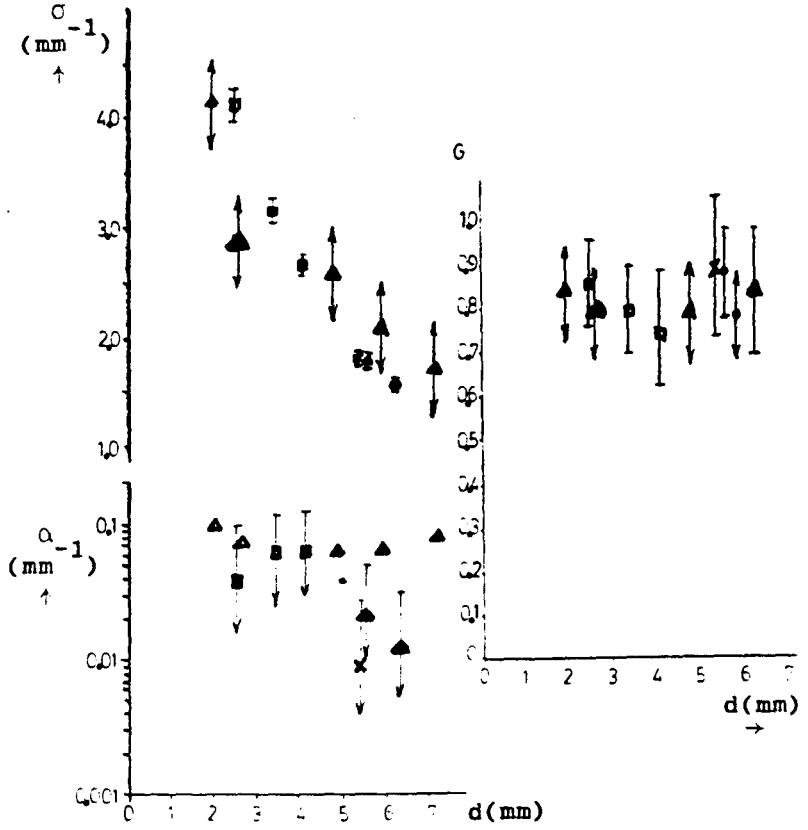

Fig. 3.2.6 α, σ *and g versus thickness (d) of sample*
Styrene butadiene: 1%,
India ink: 1% △ , 10% × , 100% □
Double integrating sphere: position A.

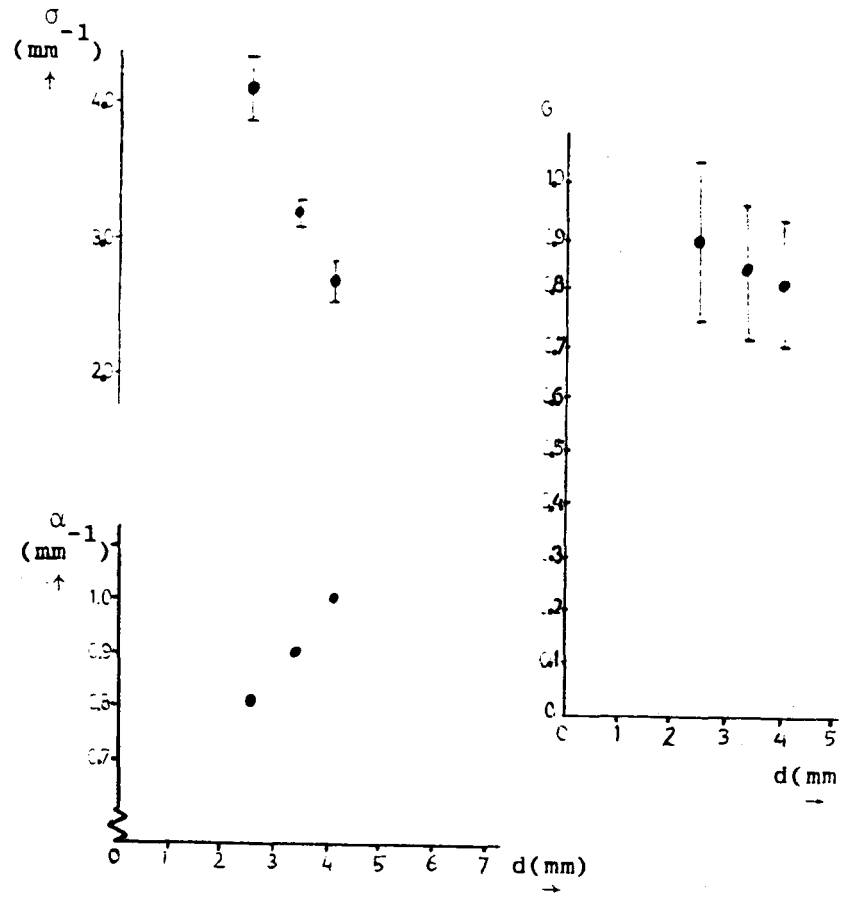

Fig. 3.2.7 α, σ *and g versus thickness (d) of sample*
Styrene butadiene: 1%, India ink:100%
Double integrating sphere: position B.

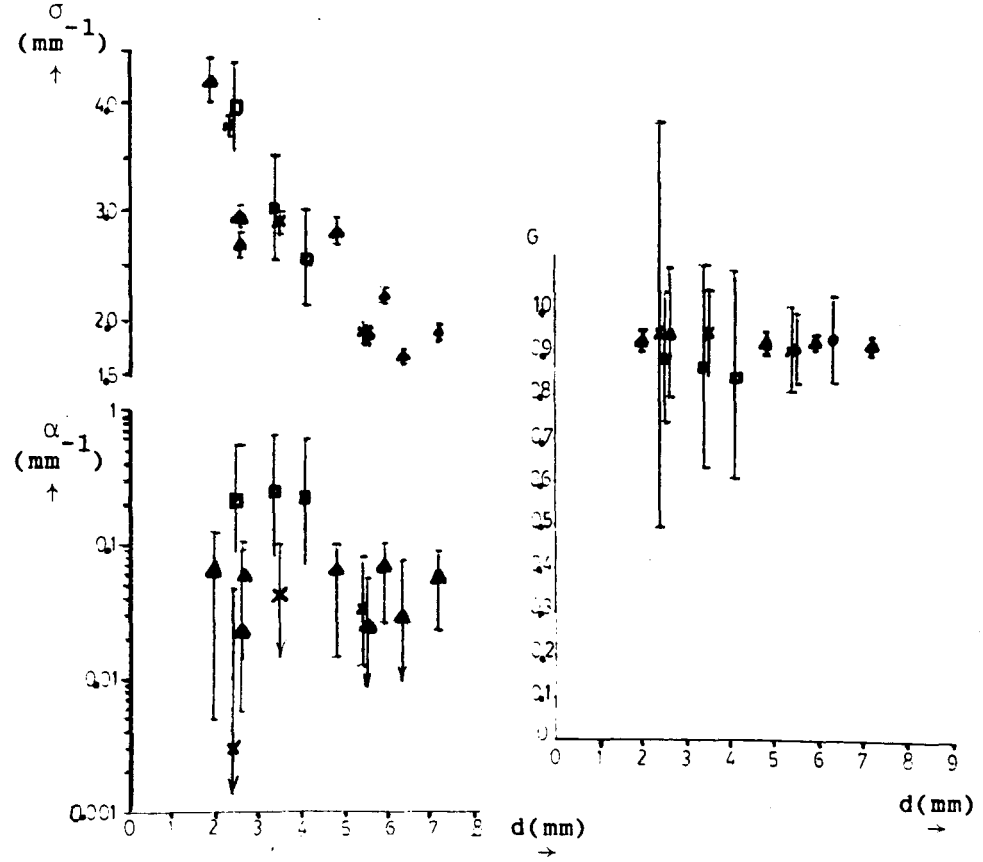

Fig. 3.2.8 α, σ *and g versus thickness (d) of sample*
Styrene butadiene: 1%, India ink
India ink: 1% ▲ , 10% × , 100% ◘ .
Single integrating sphere.

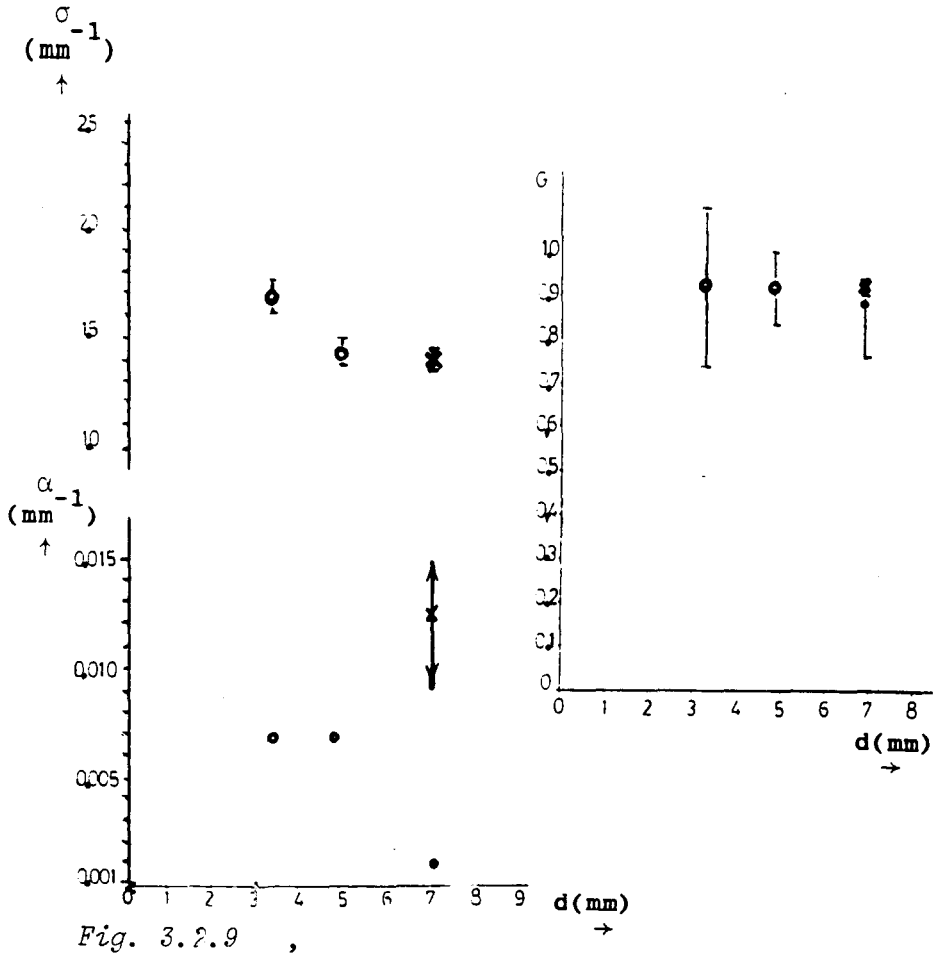

Fig. 3.2.9 ,

α, σ and g versus thickness (d) of sample
Styrene butadiene: 0.5%
India ink: 1% • , double integrating sphere, position B
1% o , 5% × , single sphere

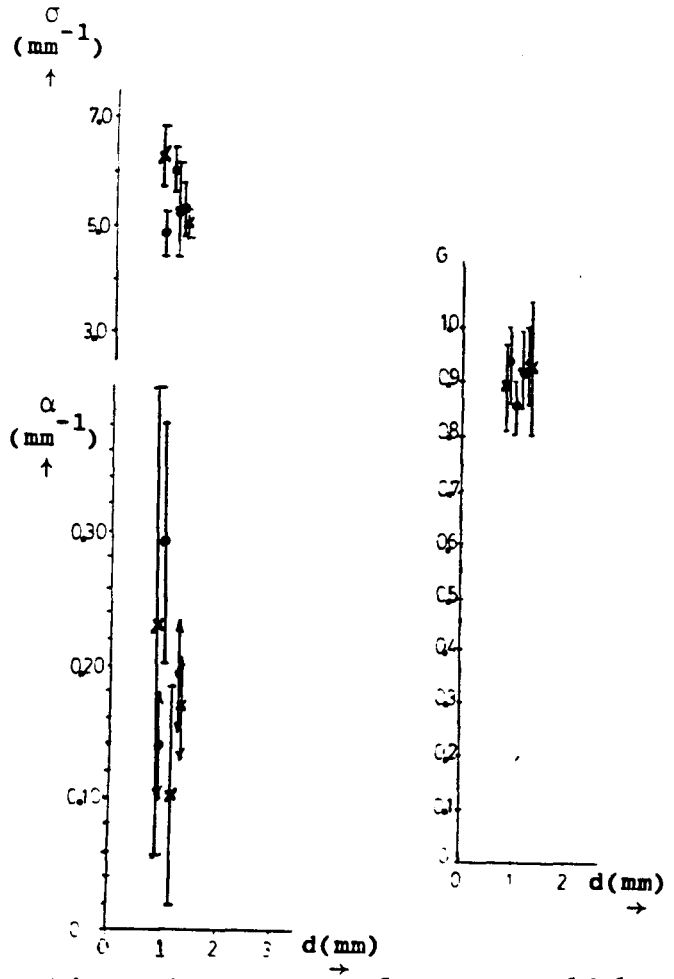

Fig. 3.2.10 α, σ *and g versus thickness (d) of sample*
Humane Brain (24 h) • ,
Canine Brain (5 h) × .
Double integrating sphere, position B.

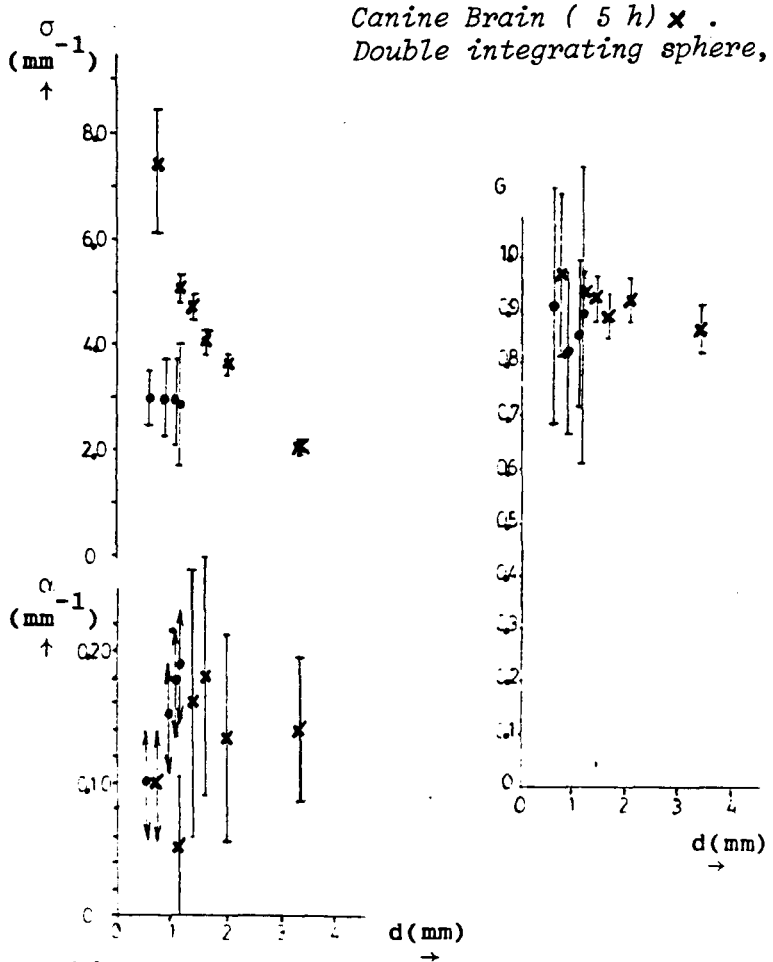

Fig. 3.2.11 α, σ *and* $\vec{g}$ *versus thickness (d) of sample*
Human Urinary bladder (24 h) • ,
Canine Bladder (2 h) × .
Double integrating sphere, position B.

Fig.3.2.6-9 show the results for styrene butadiene and indian ink, $\alpha_{\text{indian ink}} = 0.15 \pm 0.02$ mm^{-1}. Graphs 3.2.10 and 3.2.11 show the optical parameters for brain and bladder tissue from experiments done at Austin, Texas. Fig. 3.2.10 shows α, σ and g for grey matter of human and canine brain [8],[48] and fig. 3.2.11 shows the optical parameter for human and canine bladder (urothelium and mucosa) [48]. There is no significant difference in the optical parameters obtained from singel and double integrating sphere measurements. This can be explained by the fact that the light inside the samples is perfectly diffuse for the observed thickness so that index matching won't affect the light inside the sample qualitative.

3.3 The reservoir with phantom experiments.

The following experiments were performed at Rotterdam: bare fiber and isotropic detector measurements on the axis of the parallel beam. Isodose curves with isotropic detector were done at Austin. All data are presented in percentage of the incoming irradiance, which is set to 100% ($I_o = 100$), for the on axis measurement. For the light distribution curves in a phantom the isodose curves are presented relative to the incoming space irradiance which was set to 1.

The results with the bare fiber, fig.3.3.1 to 3, (opening angle FWHM 10^o) show the total attenuation coefficient of the various phantoms, from on-axis flux density gradient measurements. The following results were obtained:

From fig. 4.2.1: for 1% intralipid(10%) $\sigma = 0.704$ mm^{-1}
and for 2% intralipid(10%) $\sigma = 1.01$ mm^{-1}.
From fig. 4.2.2: for 0.5% indian ink $\alpha = 0.101$ mm^{-1}
and for 1% indian ink $\alpha = 0.206$ mm^{-1}.
From fig. 4.2.3: 0.09% styrene butadiene $\sigma = 0.132$ mm^{-1}
for 0.18% styrene butadiene $\sigma = 0.224$ mm^{-1}
and for 0.36% styrene butadiene $\sigma = 0.410$ mm^{-1}

The variation in and for the afforementioned phantoms results in the inaccuracy obtained from standard deviation calculations.

At greater depths intralipid shows deviations from an experimental attenuation due to forward scattering into the fiber (too large opening angle).

The data obtained from the on-axis measurements with an isotropic detector for an "infinite" beam (diameter 80 mm) in figures 3.3.4 to 3.3.7 give K_d

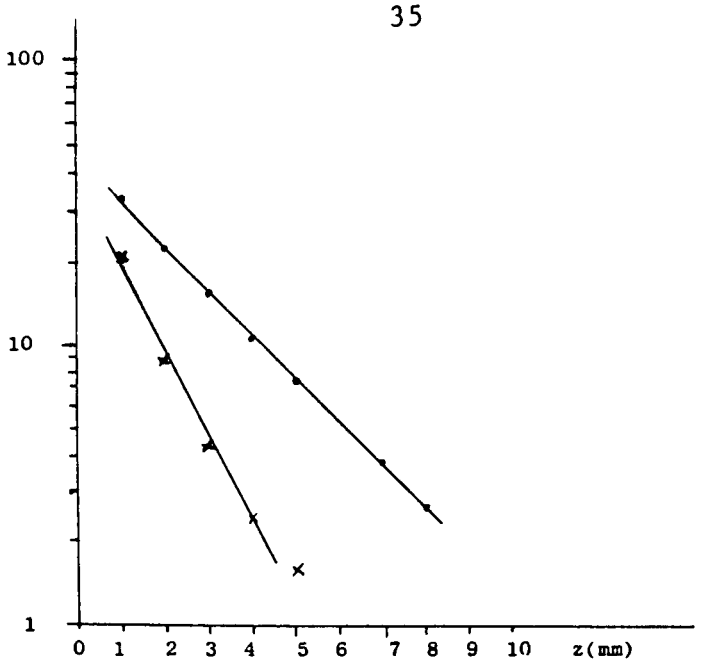

fig. 3.3.1 Gradient of radiance measured with a bare fiber in phantom. intralipid (10%): 1% • , 2% ✕ (I_o = 100)

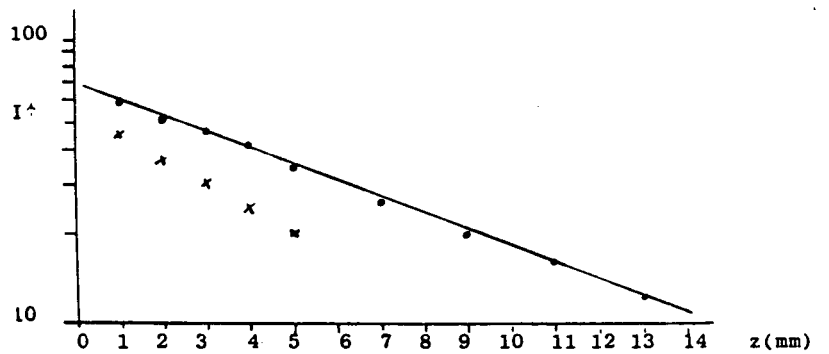

fig. 3.3.2 Gradient of radiance measured with a bare fiber in phantom. indian ink: 0.5% • , 1% ✕ (I_o = 100)

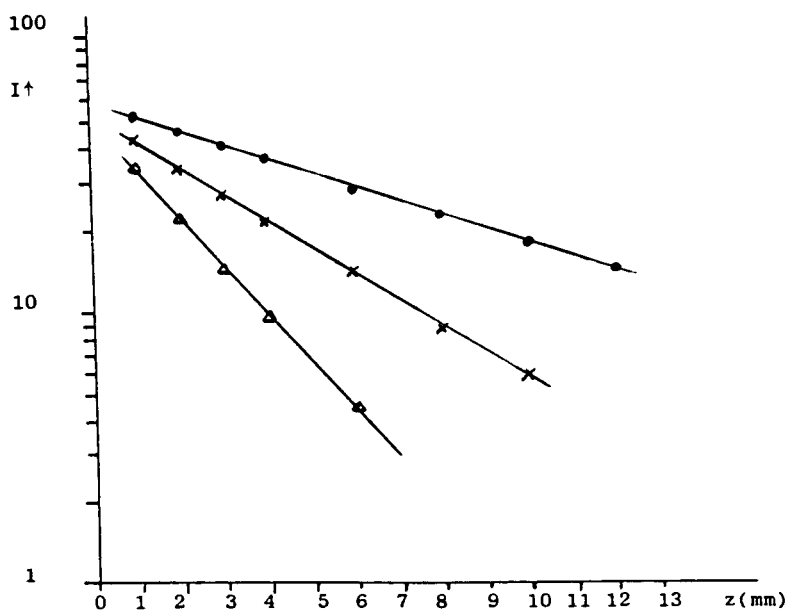

fig. 3.3.3 Gradient of radiance measured with a bare fiber in phantom. styrene butadiene: 0.09% • , 0.18% ✕ , 0.36% △ (I_o = 100)

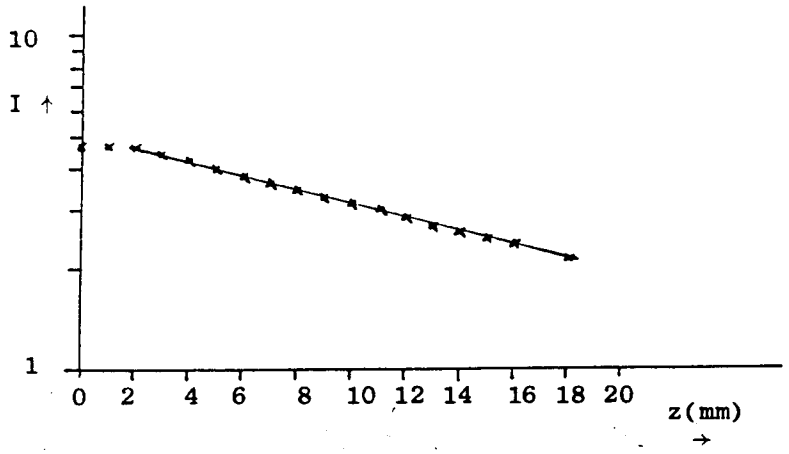

fig. 3.3.4 On axis gradient of space irradiance measured with an isotropic detector. 2% intralipid (10%) (I_o = 1)

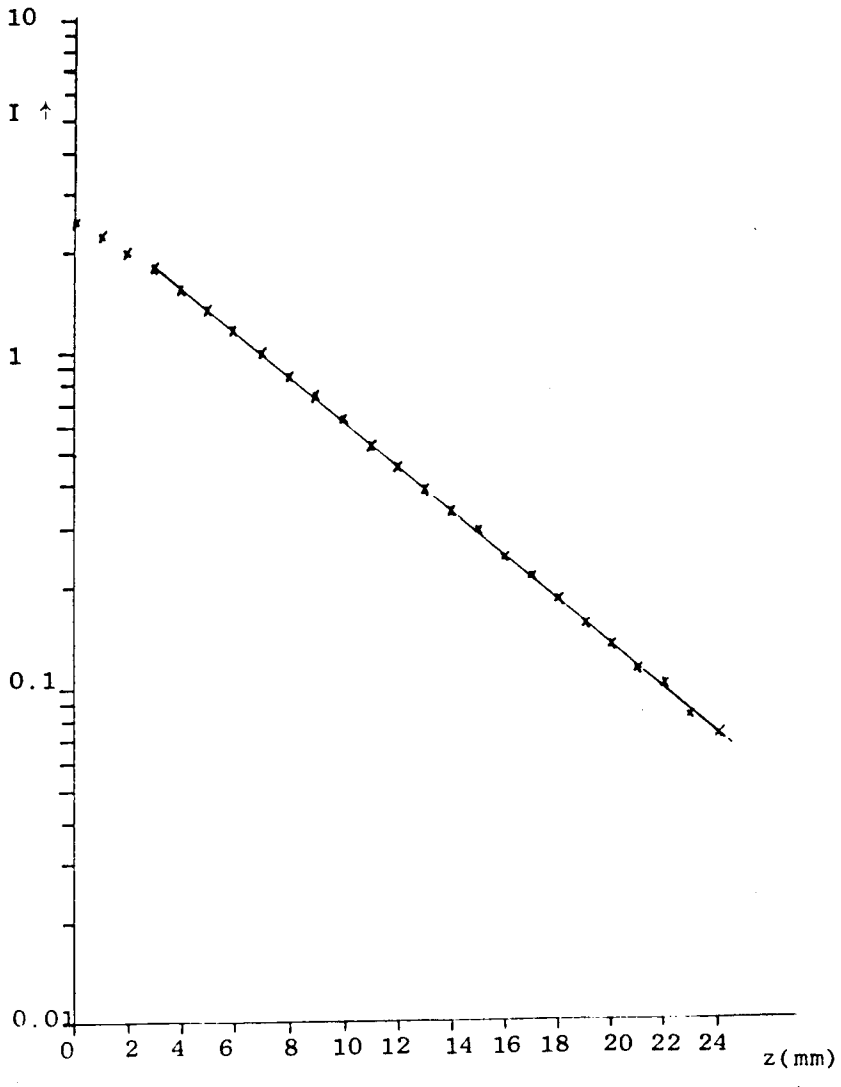

fig. 3.3.5 On axis gradient of space irradiance measured with an isotropic detector. 2% intralipid (10%), 10% indian ink (I_o = 1)

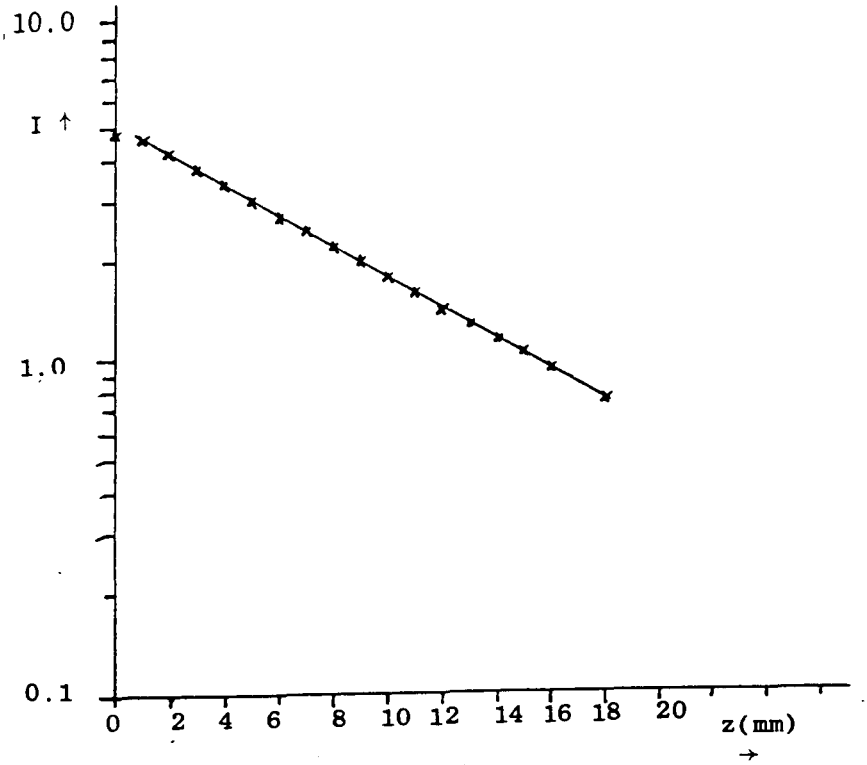

fig. 3.3.6 On axis gradient of space irradiance measured with an isotropic detector. 1% styrene butadiene, 1% indian ink (I_o = 1)

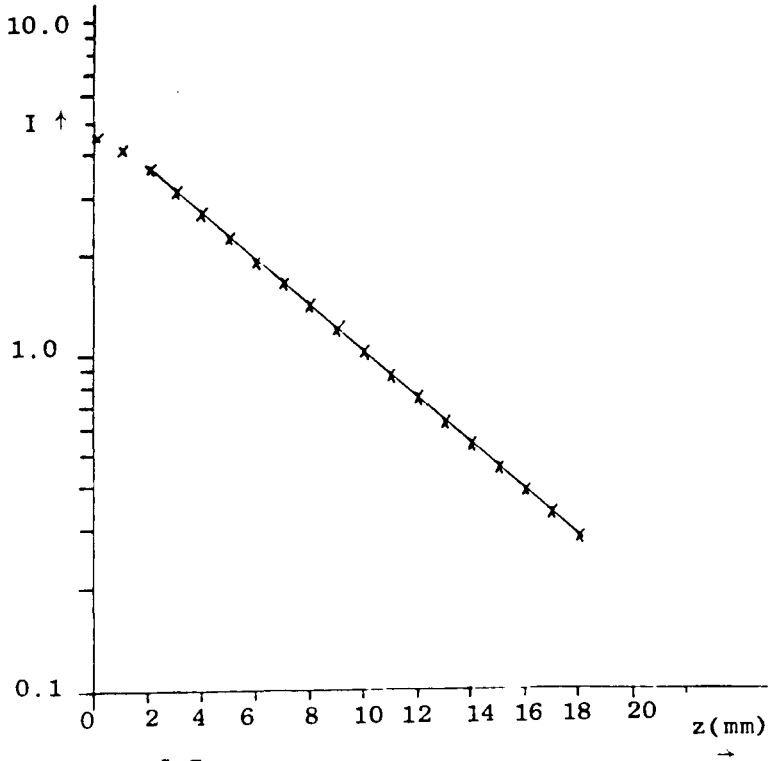

fig. 3.3.7 On axis gradient of space irradiance measured with an isotropic detector. 1% styrene butadiene, 2% indian ink (I_o = 1)

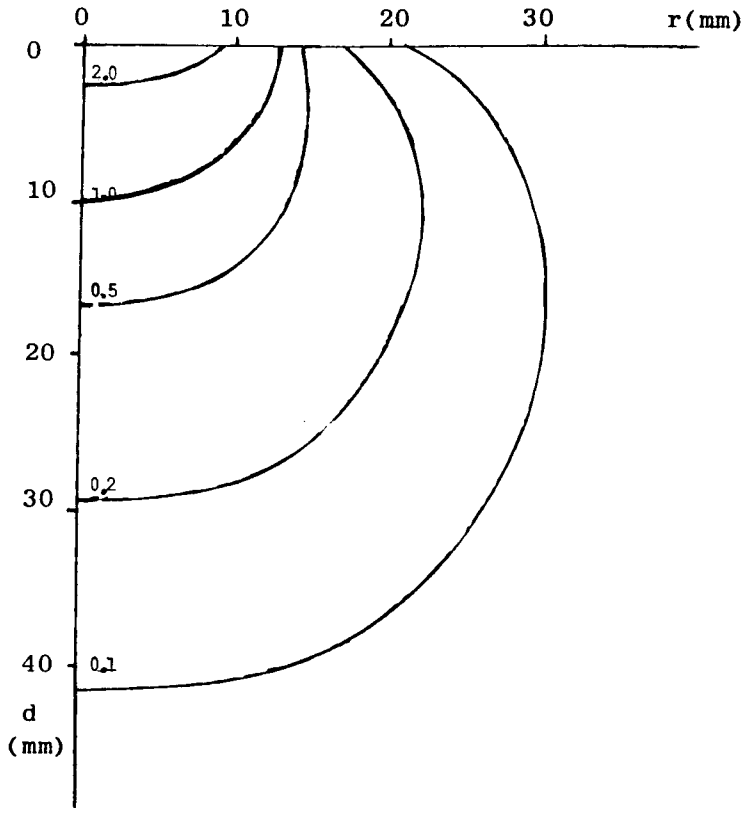

fig. 3.3.8a Space irradiance distribution from computer calculations. Isodose curves relative to $I_0 = 1$, $\sigma = 1.1\ mm^{-1}$, $\alpha = 0.002\ mm^{-1}$, $n_{medium} = 1.0$, $g = 0.83$, *beam Ø 20 mm.*

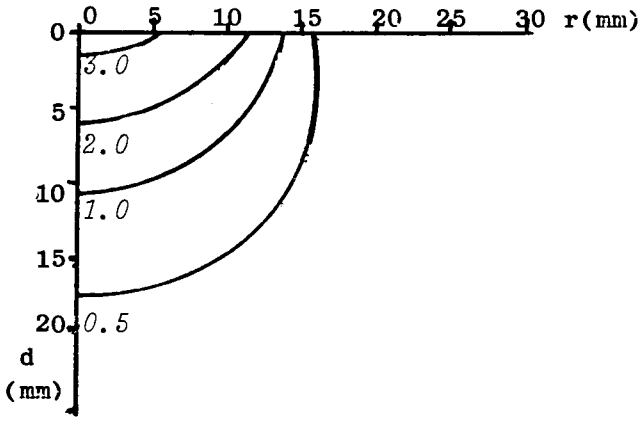

fig. 3.3.8b Space irradiance distribution from computer calculations. Isodose curves relative to $I_0 = 1$, $\sigma = 1.1\ mm^{-1}$, $\alpha = 0.002\ mm^{-1}$, $n_{medium} = 1.33$, $g = 0.83$, *beam Ø 20mm.*

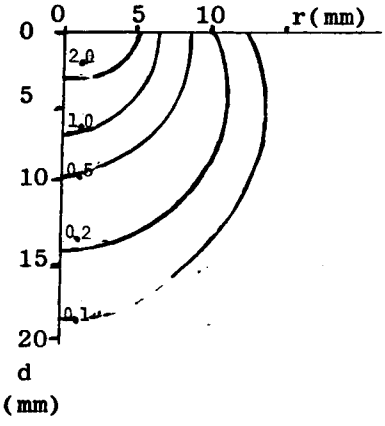

fig. 3.3.9 Space irradiance distribution fro isotropic detector measurements. Isodose curves relative to $I_0 = 1$, *2% intalipid (10%), beam Ø 20 mm.*

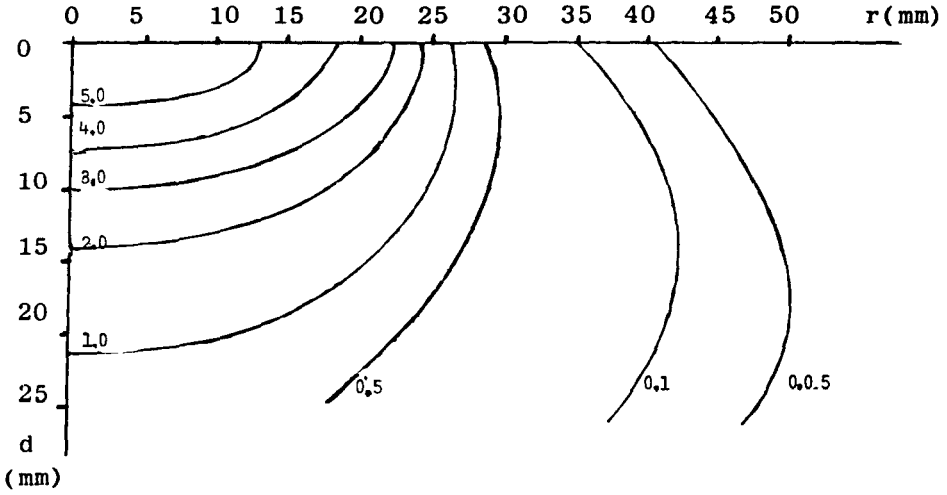

fig. 3.3.10a Space irradiance distribution from isotropic detector measurements. Isodose curves relative to I_0 = 1, 2% intralipid (10%), beam Ø 40 mm.

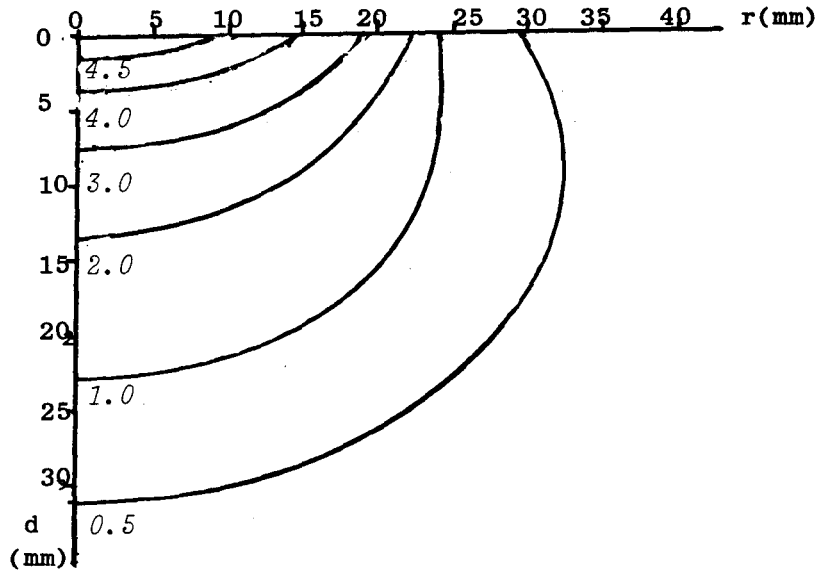

fig. 3.3.10b Space irradiance distribution from computer calculations. Isodose curves relative to I_0 = 1, σ= 1.1 mm^{-1}, α= 0.002 mm^{-1}, n_{medium}= 1.33, g= 0.83, beam Ø 40 mm.

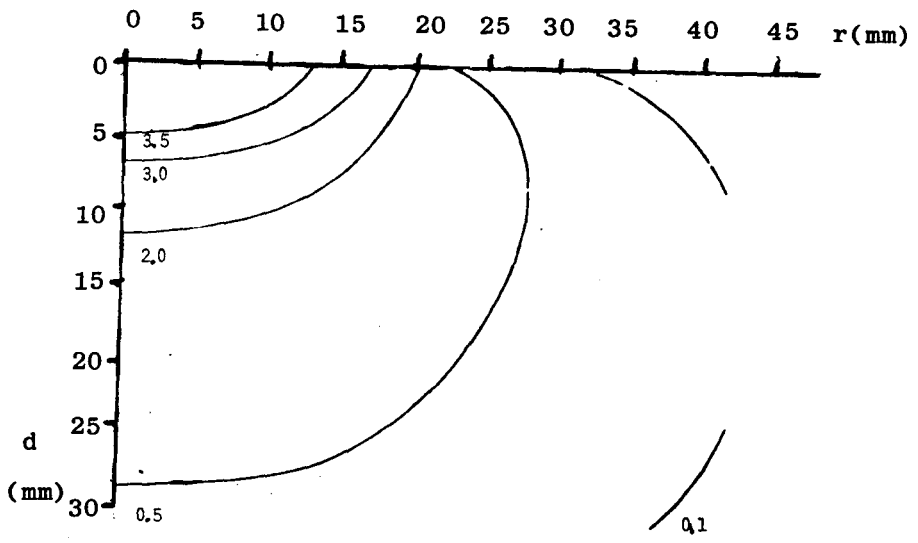

fig. 3.3.11a Space irradiance distribution from computer calculations. Isodose curves relative to $I_0 = 1$, $\sigma = 1.1\ mm^{-1}$, $\alpha = 0.002\ mm^{-1}$, $n_{medium} = 1.0$, $g = 0.83$, *beam Ø 80 mm.*

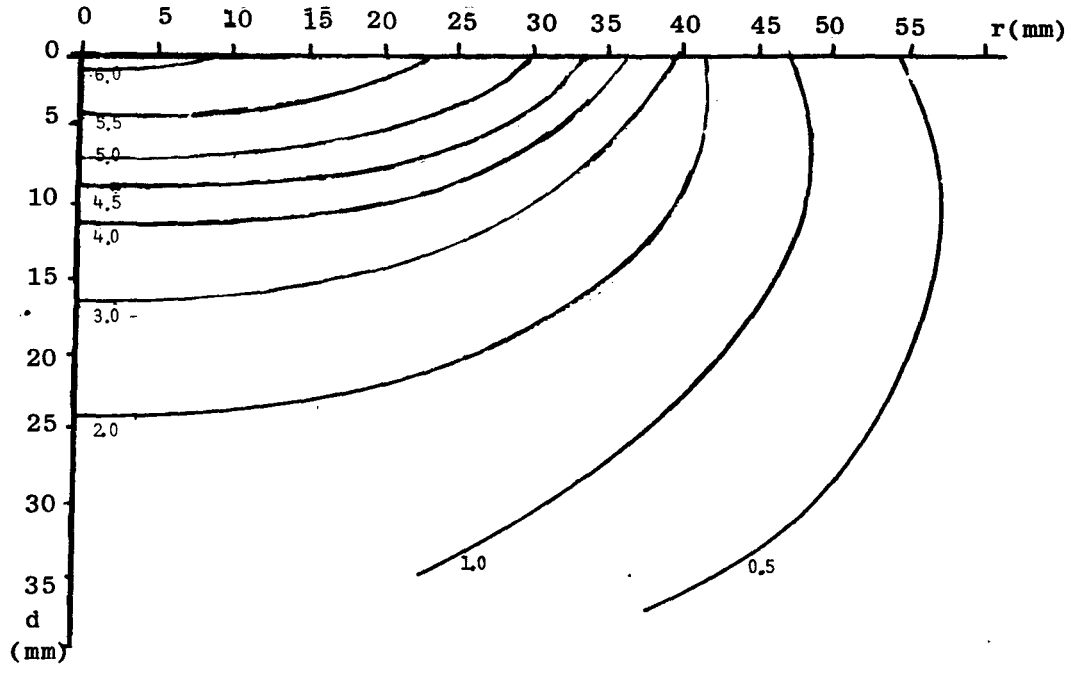

fig. 3.3.11b Space irradiance distribution from computer calculations. Isodose curves relative to $I_0 = 1$, $\sigma = 1.1\ mm^{-1}$, $\alpha = 0.002\ mm^{-1}$, $n_{medium} = 1.33$, $g = 0.83$, *beam Ø 80 mm*

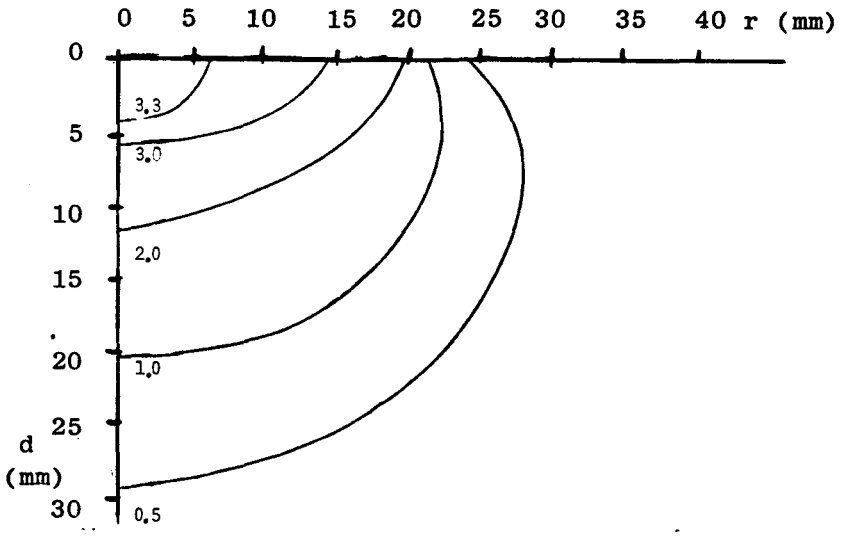

fig. 3.3.12 Space irradiance distribution from computer calculations. Isodose curves relative to $I_0 = 1$, $\sigma = 0.62\ mm^{-1}$, $\alpha = 0.002\ mm^{-1}$, $n_{medium} = 1.0$, $g = 0.83$, *beam Ø 80 mm.*

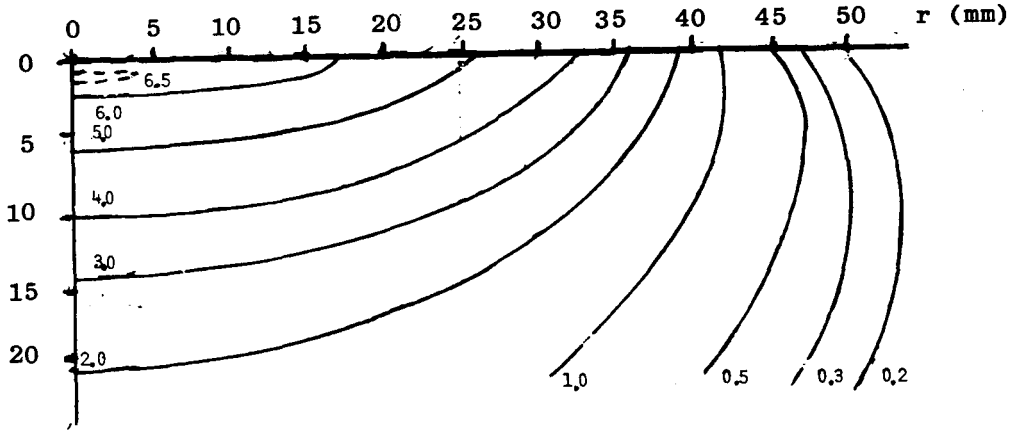

fig. 3.3.13 Space irradiance distribution from isotropic detector measurements. Isodose curves relative to $I_0 = 1$, *2% intralipid (10%), beam Ø 80 mm.*

according to equation 45. The straight line shows that the light distibution is perfectly diffuse but after two or three optical free path lenghts. The indian ink solution used had an absorption coefficient of
$\alpha_3 = 0.45 \pm 0.01$ mm^{-1}.
With $\kappa_d = 3\alpha\sigma_{tr}$, and $\sigma_{tr} = \alpha + (1-g)\sigma$ (eq.48) this will yield the following g-values from four independant measurements for each series:
2% intralipid (10%): fig. 3.3.4 $\kappa_d = 0.0500 \pm 0.0006$ mm^{-1} : g = 0.59 ± 0.09.
2% intralipid (10%) and 10% indian ink: fig. 3.3.5 $\kappa_d = 0.1563 \pm 0.0003$ mm^{-1} : g = 0.86 ± 0.03.
1% styrene butadiene and 1% indian ink: fig. 3.3.6 $\kappa_d = 0.1086 \pm 0.0002$ mm^{-1} : g = 0.26 ± 0.03.
1% styrene butadiene and 2% indian ink: fig. 3.3.7 $\kappa_d = 0.16037 \pm 0.00005$ mm^{-1}: g = 0.19 ± 0.03.
The isodose curves from spatial space irradiance measurements with the isotropic detector are shown in figs. 3.3.9 -3.3.10 and 3.3.13. Isodose curves connect positions in the phantom with identical space irradiance. Computer calculations with the computer simulation by Scott Prahl are presented in fig. 3.3.8 - 3.3.11 and 3.3.12. The experiments are done with beam diameters of 20, 40 and 80 mm. Computer calculations are presented for 20 mm, 40 mm and 80 mm beam diameter.

3.4 Goniometer experiments.

All experiments on angular dependant transmission were done at the Daniel den Hoedkliniek in Rotterdam. The graphs show the experimental results and the computer calculations from computer simulations with the program by Pascal Storchi in the so called P_9 approximation for the previously determined optical parameters. All data are normalised to 100% at 10^o to eliminate the directly transmitted beam of light through the sample. Also the graphs resulting from the nearest values found in the tables of H.C. van de Hulst where b equals thickness in optical free path lengths. In the computer calculations all values have been varied + 10% and - 5%. The absorption coefficient of indian ink is here $\alpha_3 = 20 \pm 1$ mm^{-1}

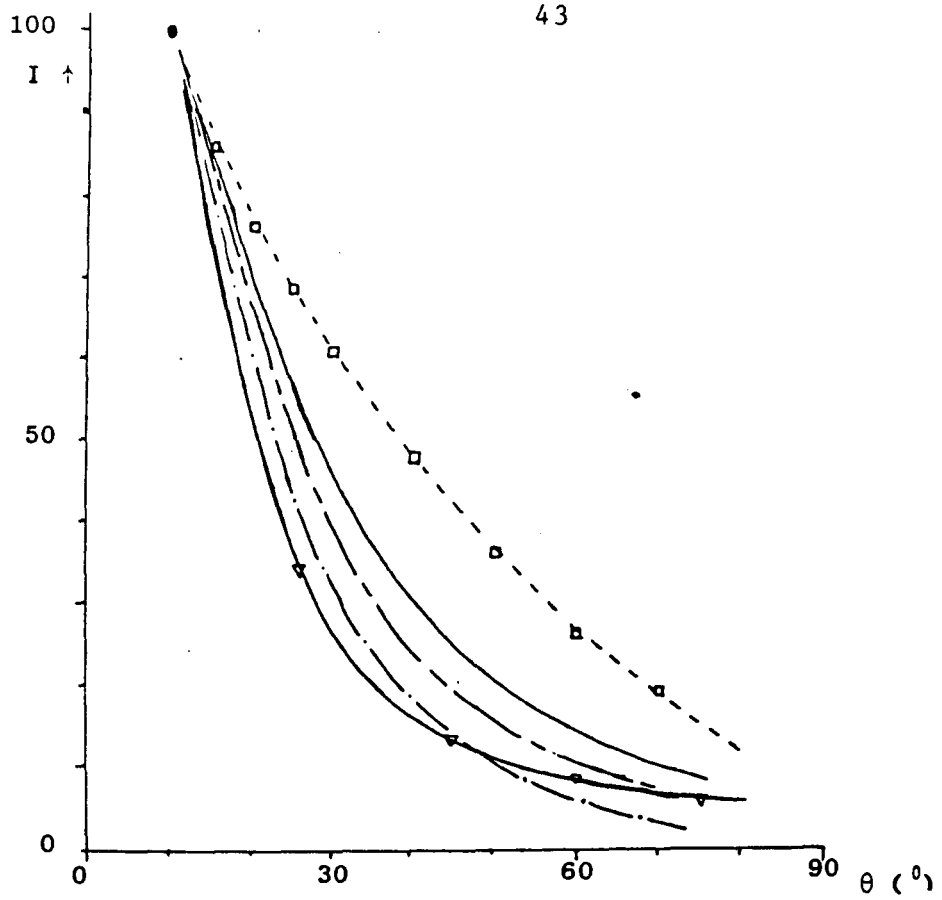

fig. 3.4.1 Angular dependant transmission; 2% Intralipid (10%). Measurements ◘ , calculations σ= 0.3mm^{-1}, α= 0.2mm^{-1}, g= 0.73 ——— , g= 0.79 — ——, g= 0.83 and g= 0.91 —·—; van de Hulst b= 2, w_0= 0.6, g= 0.75 ▽. Normalised at 10°(d=5 mm)

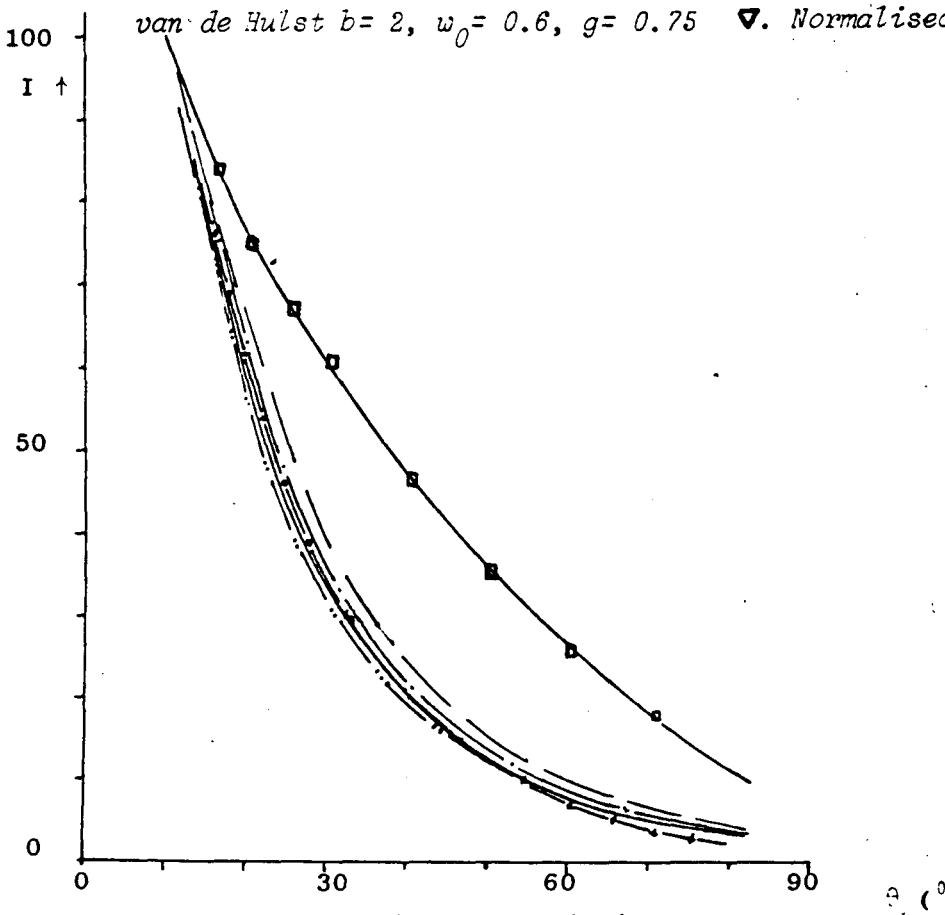

fig. 3.4.2 Angular dependant transmission; as fig. 4.3.1 only calculations σ+10% —·—, σ-5% ———, α+10% — • —, α-5% —··— ; measurements ◘ ; cal. (g=0.79) — — .

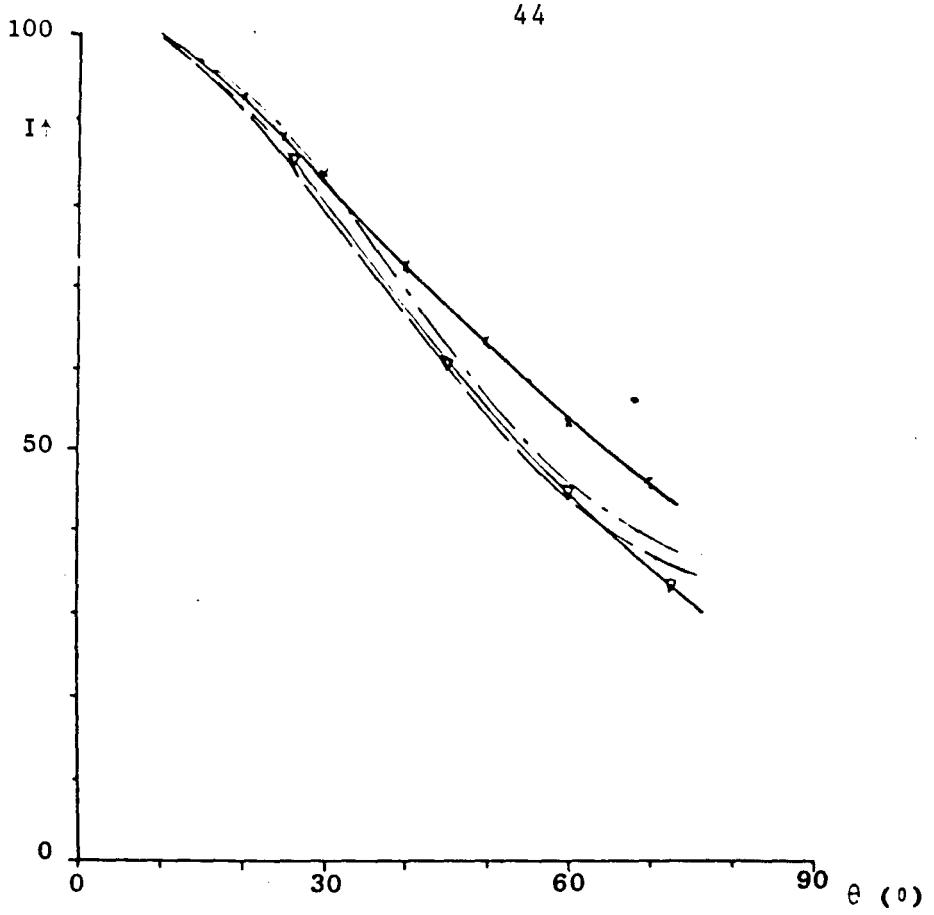

fig. 3.4.3 Angular dependant transmission; 1.3% Styrene butadiene, 0.16% Indian ink. Measurements ×, calculations σ = 0.64mm^{-1}, α = 0.16mm^{-1}, g = 0.36 and g=0.38 —·—, g=0.42 — — ; van de Hulst b= 4, w_0 = 0.8, g=0.50 ▽ . Normalised at 10° (d= 10 mm)

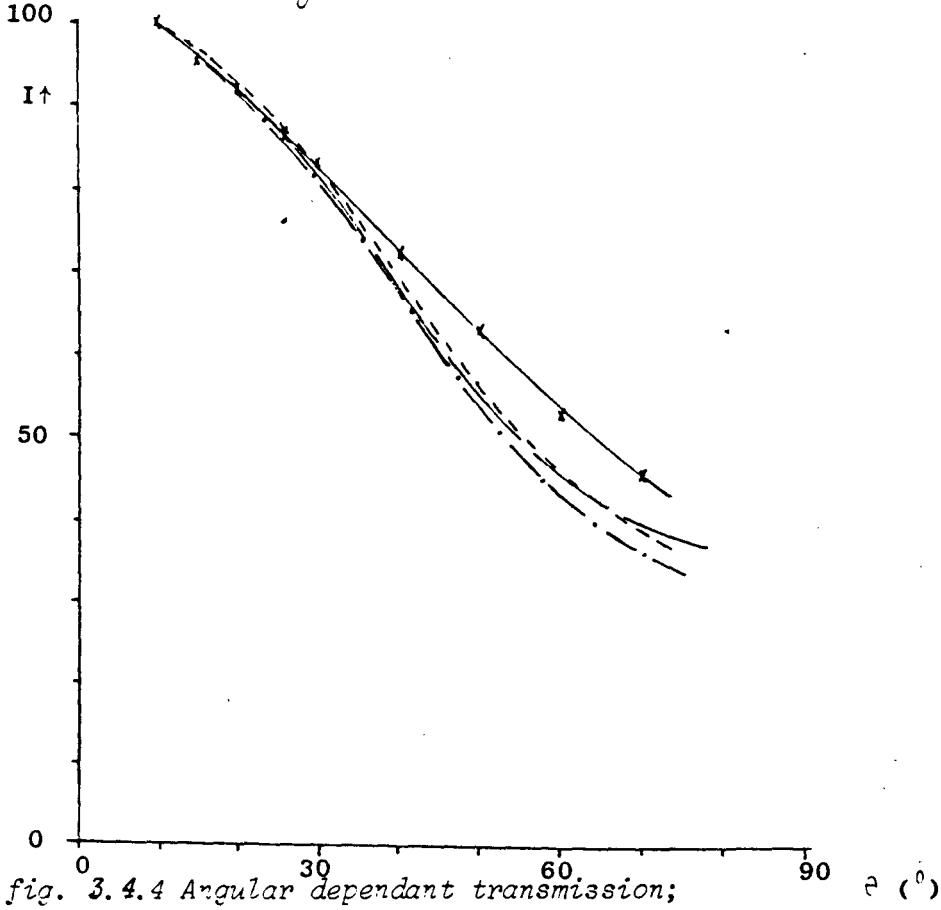

fig. 3.4.4 Angular dependant transmission; as fig. 4.3.3 only calculation σ +10% or α -5% —·—, σ -5% or α +10% ——; measurements × ; cal.: (g=0.36) - - - -.

4. Conclusions and discussion.

4.1 Introduction.

From the results presented in the previous chapter (Results), an indication on the usefulness of the presented methods and their reliability can be deduced. The single and double integrating spheres will be combined, because of the close similarity of these two methods. Next the reservoir filled with medium and the goniometer will be discussed.

4.2 The single and double integrating sphere.

As far as the integrating spheres are concerned two separate measurements should be considered. First there are the diffuse transmission and reflection measurements from the sample placed on the sphere holes: postion A and B for the double integrating sphere. Second are the collimated transmission measurements.

From fig.3.2.3,4 and 5 and fig.3.2.6,7 and 8 the following conclusions can be drawn. Measuring reflection at position B shows better agreement with the exact absorption coefficient as obtained from collimated transmission measurements. For $\alpha > 0{,}05$ mm^{-1} the order of magnitude is correct. For smaller absorption no reliable information is obtained from measuring transmission and reflection at position A or B. Also reflection from position B gives better agreement in α than from position A. Despite the high inaccuracy, the results for α, σ' and g are reproducible.
The single integrating sphere shows even better agreement in the absorption coefficient with the exact values [11], compare fig.3.2.8 with fig. 3.2.6 and fig. 3.2.5 with fig. 3.2.3. Increasing the concentrations of the absorbing medium by a factor will increase the absortion coefficient by the same factor, see e.g. fig. 3.2.2. This is observed best in the measurements with the single integrating sphere
The inaccuracy in α, σ' and g is predominantly determined by the inaccuracy in α especially for $\alpha > 0.1$ mm^{-1}.

For both the single and double integrating sphere the condition of an infinite wide slab on which the measurement analysis is based is not satisfied.

Also the condition $\alpha \ll \sigma$ is not valid in all axperiments but in most cases the results for higher α are in agreement with the exact values.
The variations in reflection coefficient for different media are small. This means that the diffuse transmission will dominate in the determination of the optical parameters in combination with the reduced collimated beam measurements.
From the collimated total attenuation coefficient [12]: q, the scattering coefficient is derived, according to eq. 40. From measurement described in paragraph 3.3 the optical properties of the ingredients of the mixture are known so there is an indication on the value of α, σ and g. The results for the scattering coefficient presented in fig. 3.2.1 and fig. 3.2.2 are too low compared to the exact values, leading to too low a values for g. In fig. 3.2.3-11 it appears that the scattering coefficient times the thickness is nearly constant for a phantom. This may point out to a systematic error. Thus also resulting in g values which are far too high compared to the expected $g<0.5$ for styrene butadiene.
One possible explanation is the occurrance of reflections from surrounding objects creating an additional bias current in the photodiode or the lock-in amplifier. The offset current/voltage of the amplifier has been carefully watched. The angle of viewing of the detector at 50 cm from the sample is problably too large in this arrangement because the aperture is to close to the detector and will capture unwanted scattered light as well as unscattered light. A suggestion for measuring the collimated total attenuation coefficient is to use a third pinhole just behind the sample. Further the possibilities of using polarisation dependent detection of the undeflected beam should be taken in consideration for future experiments, as suggested by Lars Svaasand [57].

When a laser beam is used to measure the transmission of unscattered light through a thin sample, the optical properties in the spot may change because of dehydratation. This was observed while measuring the collimated transmission of brain tissue. The transmitted radiance increased during the experiment.

4.3 Reservoir with phantom medium.

The reservoir filled with medium is used in two different ways. First, a narrow angle fiber is used that faces the incident beam and measures the on axis attenuation of the radiance. The attenuation coefficient, either α for indian ink or σ for intralipid (10%) or styrene butadiene is determined as is shown in fig. 3.3.1-3. Assuming that $\alpha >> \sigma$ for indian ink and $\sigma >> \alpha$ for intralipid (10%) and styrene butadiene. For indian ink this can be seen from the fact that there is no deviation from the experimental relation. The condition $\sigma >> \alpha$ is less easy to prove. For 2% intralipid (10) (fig. 3.3.1) a deviation from the exponential relation for on axis attenuation is observed. This is probably caused by forward scattering, resulting in forward scattered and unscattered light to be captured by the relatively large opening angle of the fiber. Second, an isotropic detector is used which measures the space irradiance either at greater depths on the axis of an infinitely wide beam, or on the axis and at radial positions from the axis for a finite incident beam. A beam diameter of 80 mm appears to be a good enough substitution for an infinite wide beam when the free optical path length is roughly equal to 1 mm. An increase in beam diameter from larger than 70 mm will have no effect on the on axis light distribution. The on axis measurements (fig. 3.3.4-7) show that at depths equal to two or three free optical path lengths the light distribution is perfectly diffuse. The exponential attenuation enables us to determine the effective attenuation coefficient κ_d, (Eq. 47). With known absorption and scattering coefficients, the scattering anisotropy factor g can be determind as well (eq. 48). It turns out to be in close agreement with what was found earlier in other experiments. The g values are in the expected range estimated from particle size [24],[44],[62] as described by Van de Hulst fig. 10.3. A beam with a diameter of 80 optical free paths lengths is assumed to be a good approximation for an infinitely wide beam: increasing the beam diameter shows no detectable change in the determination of κ_d.

The theory for an infinitely wide beam predicts an increase in space irradiance just below the liquid surface. This is also observed on the axis of the beam in experiments with a finite beam of for instance 80 free optical path lengths diameter (fig. 3.3.4 and fig. 3.3.13).

Light distribution measurements in a phantom with the isotropic detector have been compared to computer calculations for the estimated optical parameters.

For a small beam Ø 20 mm, fig. 3.3.8, fig. 3.3.9 there is a large difference in the calculated and measured isodose curves the computer calculations turn out to be an enlarged version of the experimental situation. The large diameter beam fig. 3.3.11 and fig. 3.3.12 and 3.3.13 show agreement at greater depths but the experimental situation near the surface shows much higer values and even a maximum on the axis just below the surface. The computer calculations deviate especially for small beam diameters from experimentally obtained isodose curves. This can be explained by the fact that the beam diameter is only a few optical free path length wide, and diffusion theory is probably no longer valid. The experimentally obtained maximum just below the surface [55] is in close agreement with the theoretical predicted value as a result of multiple reflection as given in equation 49.
Experimentally the size of the isotropic detector (Ø 1 mm) can influence the light distribution to be measured, when the optical free path length is too large (>1mm) or the beam diameter is very small (<1mm). This is due to the fact that the detector itself is made of scattering material. Spatial resolution is also limited by the size of the isotropic detector.

4.4 Goniometer.

Comparing the experimentally obtained angular distributions of the transmitted light through a thin sample to computer modelling (based on the computer program of Pascal Storchi) show agreement, specially for g values not too close to one. The optical parameters however can be changed without too much impact on the theoretical light distributions. Sample thicknesses may not have been sufficient to result in multiple scattering so that the light has not been perfectly diffuse. This may have caused the experiments to deviate from the computer simulations.
The calculated results are more affected by a decrease in the optical parameters than by an increase. The agreement between experimental and theoretical angular-dependance-curves is better for low values of g, compare fig. 3.4.3. with fig. 3.4.1.

Also the tables of H.C. van de Hulst give better agreement with experiments for lower g values although g = 0,38 is not tabulated, the curve shown for g = 0,5 will have a steeper slope than e.g. for g = 0,40. When the curves for decreasing g values from the tables of Van de Hulst are compared for the same

values of α, σ and thickness they tend to decrease in slope. As is expected from the meaning of the g value.

Unfortunately the tables of Van der Hulst do not cover g-values in such small steps that intrapolation of the data will give accurate values for the optical parameters that are not covered by the tables.
Measurement of the reflected light [5] as a function of the angle with the outward normal to the surface will in theory allow non-invasive determination of the optical parameters [49] by curve fitting procedures.

APPENDIX

Theory.

Equation of radiative transfer.
We examine the fundamental characteristics of the radiance in a medium containing random scattering and absorbing particles.
Consider a monochramatic bundle $d\omega$ of light energy $I(\vec{r},\vec{s})$ incident on a volume V at position r in the medium with total cross-section $(\alpha+\sigma)$, this is the combined scattering and absortion cross-section, and length ds, in the direction s´.

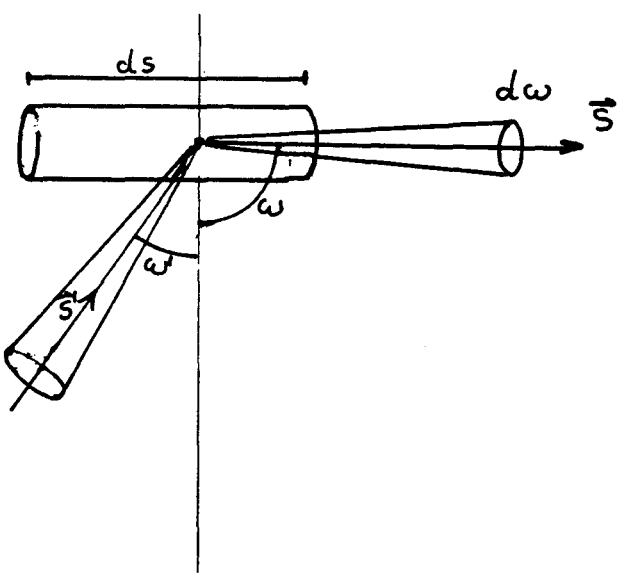

The decrease in radiance dI(r,s) for the volume V is expressed as:

$$\vec{s}.\text{grad}(I(\vec{r},\vec{s}) = -(\alpha+\sigma)\ I(\vec{r},\vec{s}) \qquad \text{(A1)}$$

At the same time the radiance increases as a result of light incident

from directions s' scattered into the direction s and is added to the radiance.

If we consider a wave incident on a scattering particle the scattered wave is gouverned by the scattering amplitude $f(s,s')$

The scattered radiance in the direction s from s' is therefore:

$$|f(\vec{s},\vec{s}')|^2 I(\vec{r},\vec{s})\,d\omega \tag{A2}$$

Adding the incident flux from all directions s' leads to:

$$dI(\vec{r},\vec{s})_{gain} = \int |f(\vec{s},\vec{s}')|^2 I(\vec{r},\vec{s})\,d\omega \tag{A3}$$

(If θ is the angle between s and s')
We can define a phase function

$$P(\vec{s},\vec{s}') = \frac{1}{(\alpha+\sigma)} |f(\vec{s},\vec{s}')|^2 \tag{A4}$$

with

$$P(\vec{s},\vec{s}')\,d = \frac{\sigma}{\alpha+\sigma} = W_0 \tag{A5}$$

W_o is called the albedo of single scattering.

A third contribution in radiance may come from a source within the medium (e.g. black body irradiation) $\mathcal{E}(r,s)$.
So the total change in radiance $I(r,s)$ can be written as:

$$\vec{s}.\text{grad}\ I(\vec{r},\vec{s}) = -(\alpha+\sigma) I(\vec{r},\vec{s}) + (\alpha+\sigma) \int I(\vec{r},\vec{s}) P(\vec{s},\vec{s}')\,d\omega' + \varepsilon(\vec{r},\vec{s}) \tag{A6}$$

The space irradiance $I(r,s)$ can be devided into
a collimated part $I_c(r,s)$ and
a diffuse part $I_d(r,s)$, $I(r,s) = I_c(r,s) + I_d(r,s)$ (A6a)

The collimated part satisfies the equation

$$\vec{s}.\text{grad } I_c(\vec{r},\vec{s}) = -(\alpha+\sigma) I_c(\vec{r},\vec{s}) \tag{A7}$$

and the diffuse part satisfies the equation

$$\vec{s}.\text{grad } I_d(\vec{r},\vec{s}) = -(\alpha+\sigma) I_d(\vec{r},\vec{s}) + (\alpha+\sigma) \int P(\vec{s},\vec{s}') I_d(\vec{r},\vec{s}) d + \varepsilon_{ri}(\vec{r},\vec{s}) + \varepsilon(\vec{r},\vec{s}) \tag{A8}$$

where $\mathcal{E}_{ri}(\mathbf{r},\mathbf{s})$ is the equivalent source function

$$\varepsilon_{ri}(\vec{r},\vec{s}) = (\alpha+\sigma) \int P(\vec{s},\vec{s}') I_c(\vec{r},\vec{s}) d\omega' \tag{A9}$$

We now turn to the diffusion approximation.
In the diffusion approximation we assume the diffuse radiance to consist of a major isotropic part and a slightly anisotropic part to account for a net flux of light

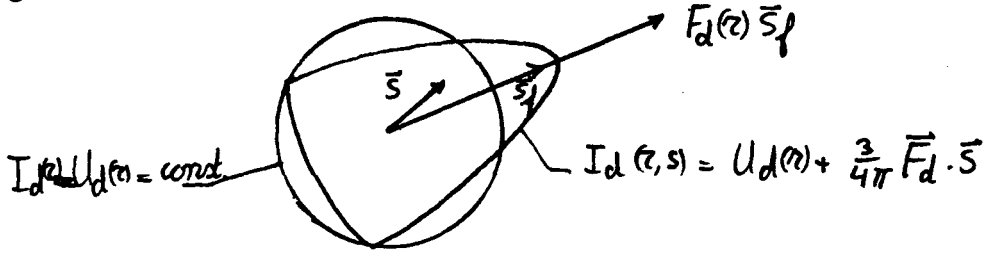

We can describe this by extending $I_d(\mathbf{r},\mathbf{s})$ in a Taylor's expansion in terms of the power of $\mathbf{s}.\mathbf{s}_f$ and stopping after the second term.

$$I_d(\vec{r},\vec{s}) = U_d(\vec{r}) + cF_d(\vec{r}).\vec{s} \tag{A10}$$

$U_d(\vec{r}) = \frac{1}{4\pi}\int I(\vec{r},\vec{s})\, d\omega$ now represents the isotropic space irradiance and (A11)

$$\vec{F_d}(\vec{r}) = \int I_d(\vec{r},\vec{s})\, s\, d\omega = F_d(\vec{r})\, s_f \tag{A12}$$

diffuse net flux
substitution of (A10) into (A12) will give c:

$$c = \frac{3}{4\pi} \tag{A13}$$

Therefore the diffuse radiance $I_d(\mathbf{r},\mathbf{s})$ is given by:

$$I_d(\vec{r},\vec{s}) = U_d(\vec{r}) + \frac{3}{4\pi} F_d(\vec{r}).\vec{s} \tag{A14}$$

We now integrate equation (A8) over all 4π of solid angle and obtain

$$\text{div } \vec{F}_d(\vec{r}) = -\alpha U_d(\vec{r}) + \sigma U_c(\vec{r}) + E(\vec{r}) \tag{A15}$$

where $$U_c(\vec{r}) = \int_{4\pi} I_c(\vec{r},\vec{s})\, d\omega \tag{A16}$$

and $$E(r) = \int_{4\pi} \varepsilon(r,s)\, d\omega \tag{A17}$$

Next substitution of (A14) into (A8) under the assumption that the phase function $P(s,s')$ is a function of the angle between s and s'.

$s.s' = \cos\gamma$ and write

$P(s.s')$ as $P(\mu,\mu')$ Ishimaru [25] (vol 2). (A18)

$\mu = \cos\theta$ θ is the angle with the positive z-axis

will lead to

$$s.\text{grad } U_d(\vec{r}) + \frac{3}{4\pi} s.\text{grad}(F_d(\vec{r}).\vec{s}) = -(\alpha+\sigma)U_d(\vec{r}) - \frac{3}{4\pi}(\alpha+\sigma)F_d(\vec{r}).s + U_d(\vec{r}) + \frac{3}{4\pi}(\alpha+\sigma)F_d(\vec{r}).sw_1 + \varepsilon_{ri}(\vec{r}) + \varepsilon(\vec{r}) \tag{A19}$$

$$w_1 = \int_{4\pi} P(\vec{s},\vec{s}')\vec{s}.\vec{s}'\, d\omega = w_o g \tag{A20}$$

$$g = \frac{\int_{4\pi} P(\vec{s},\vec{s}')\vec{s}.\vec{s}'\, d\omega}{\int_{4\pi} P(\vec{s},\vec{s}')\, d\omega} \tag{A21}$$

Equation (A19) represents the averaged forward scattering ($s.s'>0$) minus the backward scattering ($s.s'<0$) of a single particle.

The phase function $P(\mu,\mu')$ is a function of the scattering angle θ only, and can be expanded in a series of Legendre function

$$P(\mu,\mu') = 4\pi \sum_0^\infty \frac{1}{(2n+1)} w_n P_n(\mu) P_n(\mu') \tag{A22}$$

Now multiply eq. (A19) by s and integrate over all 4π of solid angle to obtain

$$\text{grad } U_d(\vec{r}) = -\frac{3}{4\pi}(\alpha+\sigma)(1-w_1)F_d(\vec{r}) + \frac{3}{4\pi}\int_{4\pi}\varepsilon_{ri}(\vec{r},\vec{s})\,s\,d + \frac{3}{4\pi}\int_{4\pi}\varepsilon(\vec{r},\vec{s})\,d \qquad (A23)$$

The quantity $(\alpha+\sigma)(1-w_1)$ is called the transport cross-section

$$\sigma_{tr} = (\alpha+\sigma)(1-w_1) = \sigma(1-g)+\alpha \qquad (A24)$$

by eliminating $F_d(r)$ equation (A23) reduced to the following:

$$\nabla^2 U_d(\vec{r}) - \kappa_d^2 U_d(\vec{r}) = -\sigma\sigma_{tr}U_c(\vec{r}) - \frac{3}{4\pi}\sigma_{tr}E(\vec{r}) + \frac{3}{4\pi}\nabla\cdot\int\varepsilon_{ri}(\vec{r},\vec{s})\,d\omega + \frac{3}{4\pi}\nabla\cdot\int\varepsilon(\vec{r},\vec{s})\,s\,d\omega \qquad (A25)$$

where $$\kappa_d^2 = 3\alpha\sigma_{tr} \qquad (A26)$$

If space has cylinder symetry and if only a plane parallel medium is being considered with the incident light coming from one side, this results in the following. All directions are related to the inward normal.
The plane parallel medium is described by x and y ordinated on the surface and by z perpendicular to the surface, z=0 at the upper air-medium interface, and the positive z direction is the inward pointing normal to this surface.

Here $\mu = \cos\theta$ (A27)
where θ is the angle with the inward normal.

The equation of radiative transfer (A8) is written as

$$\mu\frac{\partial I_d(z,\mu)}{\partial z} = -(\alpha+\sigma)I_d(z,\mu) + \int_{4\pi} I_d(z,\mu)P(\mu,\mu')\,d\mu + S(z,\mu) \qquad (A28)$$

where (A20) $S(z,\mu)$ is the source function inside the medium and will be descarded from here on

$$S(z,\mu) \equiv \varepsilon_{ri}(\vec{r},\vec{s}) + \varepsilon(\vec{r},\vec{s}) \qquad (A29)$$

The phase function is described by $P(\mu,\mu')$

$$P(\mu,\mu') = 4\pi\sum_{0}^{\infty}\frac{1}{(2n+1)}w_n P_n(\mu)P_n(\mu') \tag{A30}$$

$$\int_{-1}^{+1} P_n(\mu)P_{n'}(\mu')d\mu = \frac{2\delta_{nn'}}{2n+1} \tag{A31}$$

$$\sum_{0}^{\infty} P_n(\mu)P_n(\mu')\frac{2n+1}{2} = \delta(\mu-\mu') \tag{A32}$$

$$\frac{1}{2}\int_{-1}^{+1} P(\mu,\mu')d\mu = W_0 \tag{A33}$$

In the P_n approximation equation (A28) is multipled by P_n and integrated over 4π of all solid angle. This leads to:

$$\frac{\partial}{\partial z}\int_{-1}^{+1}\mu I_d(z,\mu)d\mu = (\alpha+\sigma)\{\int_{-1}^{+1} I_d(z,\ )+\int_{-1}^{+1}\tfrac{1}{2}d\mu\int_{-1}^{+1}P(\mu,\mu')I_d(z,\mu)d\mu'+\int_{-1}^{+1}\tfrac{1}{2}P(\mu,1)I_c(z,1)d\mu\} \tag{A35}$$

$$= -\alpha\int_{-1}^{+1} I_d(z,\mu)d\mu + \sigma I_c(z,1)$$

$$\frac{1}{(\alpha+\sigma)}\frac{\partial}{\partial z}\int_{-1}^{+1}\mu^2 I_d(z,\mu)d\mu = -\int_{-1}^{+1}\mu I_d(z,\mu)d\mu + w_1\int_{-1}^{+1}\mu I_d(z,\mu)d\mu + w_1 I_c(z,1) \tag{A36}$$

$$\frac{1}{(\alpha+\sigma)}\frac{\partial}{\partial z}\int_{-1}^{+1}\tfrac{1}{5}(3P_3+2P_1)I_d(z,\mu)d\mu = -\int_{-1}^{+1}P_2 I_d(z,\mu)d\mu + w_2\int_{-1}^{+1}P_2 I_d(z,\mu) + w_2 I_c(z,1) \tag{A37}$$

etc.

In the diffusion approximation only the first two sets of equations are used. This gives with eq. (A6a):

$$\frac{d}{dz}\int_{-1}^{+1} I_d(z,\mu)d\mu = -\alpha\int_{-1}^{+1} I_d(z,\mu)d\mu + I_c(z,1) \tag{A38}$$

$$\frac{d}{dz}\int_{-1}^{+1}\mu^2 I_d(z,\ )d = -(\alpha+\sigma)(1-w_1)\int_{-1}^{+1}\mu\ I_d(z,\mu)d\mu + (\alpha+\sigma)w_1 I_c(z,1) \tag{A39}$$

Next use eq. (A14) and introduce fluxes

$$F_{d-}(z) = 2\pi \int_0^1 \mu I_d(z,\mu)\,d\mu = 2\pi\{\tfrac{1}{2}U_d(z)+\tfrac{1}{3}F_d(z)\} \qquad \text{(A40)}$$

forward flux

$$F_{d-}(z) = -2\pi \int_{-1}^0 \mu I_d(z,\mu)\,d\mu = 2\pi\{\tfrac{1}{2}U_d(z)-\tfrac{1}{3}F_d(z)\} \qquad \text{(A41)}$$

backward flux

Equations (A38) and (A39) now reduce to

$$\frac{d}{dz}\{F_{d+}(z)-F_{d-}(z)\} = -2\alpha\{F_{d+}(z)+F_{d-}(z)\}+\sigma F_c(z) \qquad \text{(A42)}$$

$$\frac{d}{dz}\{F_{d+}(z)+F_{d+}(z)\} = -\frac{3}{2}(\alpha+\sigma)(1-w_1)\{F_{d+}(z)-F_{d-}(z)\}+\frac{3}{2}(\alpha+\sigma)w_1F_c(z) \qquad \text{(A43)}$$

Solving eq. (A42) and eq. (43) for F_d+, F_d- and F_c yields (see also eq. (A7)

$$\frac{dF_c(z)}{dz} = -(\alpha+\sigma)F_c(z) \qquad \text{(A44)}$$

$$\frac{dF_{d+}(z)}{dz} = -\{2\alpha+\frac{3}{4}(\alpha+\sigma)(1-w_1)-\alpha\}F_{d+}(z)+\{\frac{3}{4}(\alpha+\sigma)(1-w_1)-\alpha\}F_{d-}(z)+\{\frac{\alpha}{2}+\frac{3}{4}(\alpha+\sigma)w_1\}F_c(z) \qquad \text{(A45)}$$

$$\frac{dF_{d-}(z)}{dz} = -\{2\alpha+\frac{3}{4}(\alpha+\sigma)(1-w_1)-\alpha\}F_{d-}(z)+\{\frac{3}{4}(\alpha+\sigma)(1-w_1)-\alpha\}F_{d+}(z)+\{\frac{\alpha}{2}-\frac{3}{4}(\alpha+\sigma)w_1\}F_c(z) \qquad \text{(A46)}$$

GLOSSARY.

Phase function=	Scattering angle probability distribution.
Free optical path length=	Over this distance in one direction only the radiance falls to e^{-1} of its value
Irradiance=	Flow of electric magnetic radiation through a unit area. [W m^{-2}]
Flux density=	Time averaged Pointing vector [W m^{-2}].
Radiant flux density=	Time rate of flow of radiant energy per unit area [W m^{-2}].
Radiance=	Energy flow per solid angle per unit area, perpendicular to the direction of propagation [W m^{-2} sr^{-1}].
Space irradiance=	Integral of radiance over 4π solid angle [W m^{-2}]

LITERATURE.

1. Ardenne M v, Tabellen zur Angewandten Physik. VEB Deutscher Verlag des Wissenschaften, Berlin, 1973.

2. Berns MW, Lasers Surg.Med. **vol 4**, no. 1, 1984 Preface: Hematoporphyrin deriv.Photodynamic therapy.

3. Berns MW, Wilson M, Rentzepis P, Burns R, Wilz A, Lasers Surg.Med. **vol. 2**, 261-266, 1983. Cell biology of hematoporphyrin derivative (HpD).

4. Born M, Wolf E, 1964, Principles of Optics, Macmillan, New York.

5. Brinkworth BJ, Appl.Opt., 11, 1434, 1972, Interpretation of the Kubelka-Munk coefficients in reflection theory

6. Chandrasekhar S, Radiative transfer, 1950, Oxford Univ.Press, London and New Yrok and Dover, New York 1960

7. Doiron DR, Gomer CJ. Progress in Clinical and Biological Research, vol. 170, 1983. Porphyrin Localisation and treatment of tumours. Alan R. Liss Inc. New York, 133-148.

8. Donald HF, Schade JP. Atlas of the human brain. Elsevier Publishing Comp., Amsterdam, London, New York, 1966.

9. Dreosti GM, Absorptie en verstrooiing van lig in melkglas, Willemse Utrecht, 1930.

10. Egan WG, Hilgeman T, Applied Optics **vol. 14**, no. 5 1137-1142, May 1975, Integrating sphere for measurements between 0,185 μm and 12 μm

11. Flock ST, Wilson BC, Patterson MS, Total attenuation coefficients and scattering phase functions of tissues and phantom materials at 633 nm. Med.Physics, in press 1987.

12. Funk CJ, Appl.Opt. 12, 301-313, 1973, Multiple scattering calculations of light propagation in ocean water.

13. Gate LF, Appl.Opt. vol. 13, 2, 1964, Comparison of the photon diffusion model and Kubelka-Munk equation with the exact solution of the radiative transfer equation, 1974.

14. Gemert MJC v, Cheong WF, Welch AJ, Star WM, Light delivery for whole bladder photodynamic therapy, Lasers Med.Science (in press 1987).

15. Gemert MJC v, Huulsbergen Henning JP, Arch.Dermatol.Res. 270, 429-439, 1981, A model approach to laser coagulation of Dermal Vascular Lesions.

16. Gemert MJC van, Star WM, Lasers Life Sci. (in press 1987). Relations between Kubelka-Munk and transport optical parameters for anisotropic scattering.

17. Gemert MJC van, Welch AJ, Star WM, Prahl SA, Motamedi M, Cheong WF, Tissue optics for a slab geometry in the diffusion approximation. Lasers Med.Science .(In press 1987.)

18. Gijsbers GHM, thesis VDF-NK83

19. Goedecke GH, J.Opt.Soc.Am. **vol. 67**, no. 10, 1339-1348, October 1977, Radiative transfer in closely packed media.

20. Groenhuis RAJ, Ferwerda HA, Ten Bosch JJ, Applied Optics, vol. 22,24, 2456-2462 (1983).

21. Groenhuis RAJ, Ferwerda HA, Ten Bosch JJ, Applied Optics, vol. 22,24, 2463-2467 (1983).

22. Grossweiner LJ, Lasers Surg.Med, 6, 462-466, 1986, Optical Dosimetry in Photodynamic Therapy.

23. Gurevic M, Physik. Zeitschr. XXXI, 1930, 753-763, Rationelle Klassifikation der lichtstreuenden Medien.

24. Hulst HC van der, Multiple Light scatt. **vol. 2**, 1 & 2.

25. Ishimaru A, Academic Press New York and San Francisco and London, New York, 1978, **vol. 1-2**, Wave propagation and scattering in random media.

26. Jackson JD, Classical electrodynamics. Second edition. (1975). John Wiley & Sons Inc.; New York, London, Sydney, Toronto.

27. Jacques JA, Kuppenheim HF, Journal of the optical soc. of America **vol. 45**, no. 6, 1955, 460-470: Theory of the integrating sphere.

28. Jacques SL, Prahl SA, Lasers Surg. Med. Modelling optical and thermal distributions in tissue during laser irradiation. In press 1987.

29. Jacquez JA, Kuppenheim HF, J.Opt.Soc.Am., **vol. 45**, no. 6 460-47 , July 1953, Theory of the integrating sphere.

30. Johson CC, IEEE transactions on bio-medical engineering, **vol. BME 17**, no. 2, april 1970, 129-133. Optical diffusion in blood.

31. Kato H, Aizawa K, Lasers Surg.Med. **vol. 4**, no. 1, 1984, 49-58. Clinical measurement of tumor fluorescence using new diagnostic system with hematoporphyrin derivate, laser photo-radiation and a spectroscope.

32. Kerker M, Academic Press, New York, H3, The Scattering of Light.

33. Klier K, J. Opt.Soc.Am. **vol. 62**, no. 7, 882-885 July 1972, Absorption and scattering in Plane parallel Turbid Media.

34. Kottler F, Journal of the optical Soc. of America **vol.50**, no. 5, 483-490, 1960. Turbid media with plane-parallel surfaces.

35. Kottler F, Progress in opties, 3: 3-28, 1964, The elements of radiative transfer.

36. Kubelka P, J. Opt Soc. Am. **vol. 38**: 448-457, 1948, New contribution to optics in intensely Scattering Materials, Part I.

37. Kubelka P, Journal of the optical society of America, **vol. 44**, no. 5, 1954, 330-335, New contribution to the optics in intensely Scattering Materials, Part II.

38. Landolt-Bornstein, Zahlenwerte und Funktionen aus Physik.Chemie-Astronomie-Geophysik-Technik (1980), Springer-Verlag, Berlin Heidelgerg New York.

39. Lipson RL, Baldes EJ, Olsen AM, Journal of the National Cancer Institute **vol. 26**, no. 1, Jan. 1961, 1-11: The use of a derivative of hematoporphyrin in tumor detection.

40. Marijnissen JPA, Splinter R, Storchi PRM, Star WM, Keyzer M, Gemert MJC v, Determination of the optical properties of tissues: comparison of two methods, poster ELA Conference Amsterdam, November 1986.

41. McCaughan JS, Guy JT, Hawley P, Hicks W, Inglis W, Lasers Surg.Med. **vol.3**, 199-209, 1983. Hematoporphyrin-derivative and Photoradiation therapy of malignant tumors.

42. McKenzie AL, Carruth AS, Phys.Med.Biol. **vol. 29**, 6, 619-641, 1984, Lasers Surg.Med.

43. McKenzie AL, Phys.Med.Biol. **vol. 29**, 1, 53-56, 1984, How to control beam profile during laser photoradiation.

44. Mie G, Ann. Physik 4, 25, pp. 377, 1908.

45. Miller OE, Sant AJ, Journal of the optical Society of America, **vol. 48**, no. 11, november 1958, 828-831, Incomplete integrating sphere.

46. Mudgett PS, Richards LW, Applied Optics, **vol. 10**, no. 7, 1485-1501, July 1971, Multiple Scattering Calculations for Technology.

47. Nelson JS, Chung-Ho SC, Berns MW, Lasers Surg.Med. **vol. 6**, 131-136, 1986, Study of in vivo and in vitro photosensitizing capabilities of Uroporphyrin I compared to Photofrin II.

48. Netter FH, The Ciba Collection of Medical Illustrations, 1970, vol. 2: Reporductive System
1967, vol. 1: Nevous System.
Colorpress, New York.

49. Patterson MS, Wilson BC, Foather JW, Burns DM, Pushka W, Photochem. Photobiol (in press 1987). The Measurement of dihematoporphyrin ether concentration in tissue by reflectance spectrophotometry.

50. Prahl SA, Proposal to investigate three-dimensional calculations of light distribution in tissue. (privat communication)

51. Preston JS, Transactions of the optical society, **vol. 31**, 15-35, 1930. The reflection factor of magnesium oxide.

52. Putten WJM vd, Gemert MJC v, Phys.Med.Biol. **vol. 28**, no. 6, 639-645, 1983, A modelling approach to the detection of subcutaneous tumours by haematoporphyrin-der.fluorescence.

53. Sandeman DR, Lasers in Medical Science, **vol. 1**: 163-174 (1986). Photodynamic therapy in the management of malignant gliomas: a review.

54. Schwarzschild K, Sitz. Ber. Preuss. Akad. Wiss Berlin 1183, 1914.

55. Star WM, Marijnissen JPA, Berg-Blok AE vd, Treurniet-Donker AD, Reinhold HS, Klinische Fysika, 80-88, 1985

56. Star WM, Marijnissen JPA, Gemert MJC v, Jansen H, Light dosimetry for photodynamic therapy by whole bladder wall irradiation.

57. Svaasand LO, Boerslid T, Oeveraasen, Laser Surg.Med., 5: 584-602, 1985, Thermal and optical properties of living tissue.

58. Turner L, Rayleigh-Gouss.Born, Light scattering by ensembles of randomly oriented anisotrpic particles, Appl.Opt. 12, 1085-1090.

59. Verdaasdonk R, Bepaling van optische coefficienten van biologische weefsels, stageverslag, 1984, University of Technology Eindhoven, Eindhoven, The Netherlands.

60. Wilson BC, Patterson MS, Burno DM, Lasers Med. Science (in press 1987), The effect of photosensitizer concentration in tissue on the penetration depth of photoactivating light.

61. Wilson BC, Patterson MS, Phys.Med.Biol. 1986 **vol. 31**, no. 4, 327-360: The physics of photodynamic therapy.

62. Yeh C, Phys.Rev. 135, A1193-A1201, 1964, Perturbation approach to the diffraction of electromagnetic waves by arbitrarily shaped dielectric obstacles.

63. Zerlaut GA, Andersen TE, Applied Optics **vol.20**, no. 21, 3797-3804, November 1981, Multiple-Integrating sphere spectrophoto-meter for measuring absolute spectral reflectance and transmittance.